NTNU – Trondheim
Norwegian University of
Science and Technology

Fatigue of Flexible Risers Considering Alternative Constitutive Models

Tom Are Grøv

Marine Technology
Submission date: June 2014
Supervisor: Svein Sævik, IMT

Norwegian University of Science and Technology
Department of Marine Technology

NTNU Trondheim
Norges teknisk-naturvitenskapelige universitet
Institutt for marin teknikk

MASTER THESIS SPRING 2014

for

Stud. tech. Tom Are Grøv

Fatigue of Flexible Risers considering alternative constitutive models

Utmatting av fleksible rør med bruk av alternative materialmodeller

Flexible pipe response is governed by significant hysteresis in the bending mode related to friction between layers. To perform global dynamic analysis this can be handled in two ways:
1. Using the physically correct non-linear moment curvature representation of the pipe in the global model leading to long simulation times
2. Establish an equivalent viscous damping coefficient and use a linear global model

The project work focus on models for investigation the above and is to be carried out as proposed below:

1. Literature study, including flexible pipe technology focusing on the mechanical response and associated design criteria. This is also to include the techniques used to perform global and local response analysis (ensuring that the relevant design criteria are met) including non-linear finite element methods and non-linear time-domain analysis techniques with focus on the methods applied in computer programs such as ORCAFLEX, RIFLEX, SIMLA and BFLEX.
2. Define a riser scenario in terms of water depth, vessel geometry, vessel RAO, pipe cross-section properties, hydrodynamic coefficients and environmental conditions.
3. Define a cross-section model in Bflex to calculate the cross-section characteristics in terms of axial-force versus strain, torque version torsion and moment versus curvature as a function of water depth.
4. Establish alternative models in SIMLA assuming linear and non-linear moment-curvature relations and perform non-linear, regular wave dynamic analysis to investigate the dynamic responses in terms of curvature and tension variations for a variety of wave classes.
5. Perform fatigue analysis and compare the results from applying the inputs from the two alternative models at different locations along the riser.
6. Perform the analysis using irregular waves and the scatter diagram.
7. Conclusions and recommendations for further work

Input data is assumed to be provided by 4Subsea.

The work scope may prove to be larger than initially anticipated. Subject to approval from the supervisors, topics may be deleted from the list above or reduced in extent.

In the thesis the candidate shall present his personal contribution to the resolution of problems within the scope of the thesis work

Theories and conclusions should be based on mathematical derivations and/or logic reasoning identifying the various steps in the deduction.

The candidate should utilise the existing possibilities for obtaining relevant literature.

Thesis format
The thesis should be organised in a rational manner to give a clear exposition of results, assessments, and conclusions. The text should be brief and to the point, with a clear language. Telegraphic language should be avoided.

The thesis shall contain the following elements: A text defining the scope, preface, list of contents, summary, main body of thesis, conclusions with recommendations for further work, list of symbols and acronyms, references and (optional) appendices. All figures, tables and equations shall be numerated.

The supervisors may require that the candidate, in an early stage of the work, presents a written plan for the completion of the work.

The original contribution of the candidate and material taken from other sources shall be clearly defined. Work from other sources shall be properly referenced using an acknowledged referencing system.

The report shall be submitted in two copies:
- Signed by the candidate
- The text defining the scope included
- In bound volume(s)
- Drawings and/or computer prints which cannot be bound should be organised in a separate folder.

Ownership
NTNU has according to the present rules the ownership of the thesis. Any use of the thesis has to be approved by NTNU (or external partner when this applies). The department has the right to use the thesis as if the work was carried out by a NTNU employee, if nothing else has been agreed in advance.

Thesis supervisor:

Prof. Svein Sævik, NTNU

Deadline: June 10th , 2014

Trondheim, January, 2014

Svein Sævik

NOTE: In agreement with the supervisor, the following two modifications were done: Only one irregular sea-state was applied. No equivalent viscous damping was used in the linear models. (Written by the student).

Preface

This report is written as a result of a final project carried out during the 10^{th} semester at the Norwegian University of Science and Technology (NTNU). It is written for the degree of Master of Science in Marine Structures, at the Department of Marine Technology. The work took place in Trondheim, during Spring 2014.

The interest in flexible risers came during a summer internship after fourth grade. Since then, the riser's complex construction and distinctive behaviour has appealed to me. Working with this thesis has increased my understanding about its behaviour and how to approach scientific problems.

I would like to thank my supervisor Professor Svein Sævik for his enthusiasm and great knowledge about this topic. His availability and expertise on the programs used in this thesis has made it easy to get help. I would also like to thank my future employer 4Subsea for providing me with a riser system to use in the analyses.

Trondheim, June 10, 2014

Tom Are Grøv

Summary

The flexible riser is made up of both polymeric layers and steel layers, including steel tendons. Due to internal pressure and tension of the pipe, the tendons act with a normal force on the layer underneath. In the beginning when the riser is being bend, the frictional force will prevent the layers from slipping. However, for a given bending moment, these layers slip. This interaction between the layers results in a non-linear response.

The main purpose of this thesis was to investigate on the dynamic response and fatigue estimate when taking this non-linear behaviour into account. Most of today's current practice assumes a linear behaviour with a low bending stiffness, resulting in an overly conservative estimate.

To examine this non-linear response, three different material models were established: One non-linear model, representing the stick-slip effect due to friction between the layers, and two linear models. The linear models differ in which stiffness was used: Either the stiffness corresponding to when the pipe is depressurised, or when it is fully pressurised and assuming that the pipe layers cannot slip.

The process was carried out in the following way: First, the global response of a flexible riser was calculated. This was done for each of the three models, and the tension and curvature history was printed out. This was used as input to a detailed local model, which was able to calculate the stresses in the tendons along the cross section. Based on the stress history, the fatigue damage was calculated. The response for regular waves heading in plane and in 45 degrees was checked, along with one irregular sea-state.

The non-linear model estimated a yearly damage about 25% higher than the linear stick-stiffness model. The linear slip-stiffness model, which is the model closest to today's practice, predicted a damage 7 times greater than the non-linear model. This model seems to predict an overly conservative answer both in terms of the dynamic response and the fatigue damage. With regard to the time consumption, the non-linear model took about three times longer to complete. By using a dedicated analysis computer, a full irregular analysis could be done in about four days.

The increased motion of the vessel when waves were heading in 45 degrees led to an earlier slip of the layers. This led to a slightly higher difference in damage

between the non-linear and the linear slip-stiffness model. Thus, hysteresis seems to be more critical when the waves lead to motion about all axes, given that the waves are equal.

These results showed that taking the non-linear stick-slip effect into account could significantly reduce the predicted damage, compared to using the overly conservative linear slip-stiffness model. This can be applied to prove that designs, which before was deemed unviable by using a linear model, is safe with respect to fatigue. This opens up for the use of lower-cost solutions while still proving the design to be safe. With the performance of today's computers, taking this stick-slip effect into account is a realistic option.

Sammendrag

Fleksible stigerør er består av lag med polymerer og stål, inkludert strekkarming. På grunn av det høye trykket og strekkreftene i stigerøret virker det normalkrefter på de ulike lagene. I starten når røret blir bøyd, vil denne friksjonskraften hindre at lagene slipper. Hvis bøyemomentet overskrider en gitt verdi, vil lagene likevel slippe, noe som fører til at stivheten til røret blir mindre. Denne effekten fører til en ikke-linear respons.

Hensikten med dette prosjektet var å undersøke den dynamiske responsen samt utmattingsskaden når man tok hensyn til denne ikke-lineære oppførselen. Dagens metode består av å anta en linear oppførsel med en lav bøyestivhet, noe som resulterer i et konservativt estimat.

For å undersøke denne ikke-lineære responsen ble tre forskjellige materialmodeller etablert: En ikke-lineær modell, som representerer denne stikk-slipp effekten mellom lagene, og to lineære modeller. De lineære modellene er forskjellige med tanke på hvilke bøyestivhet som er brukt: Enten ble stivheten som korresponderte til når det ikke er friksjonskrefter brukt, eller når man antok at lagene ikke kunne slippe.

Følgende metode ble brukt: Først ble en global analyse av stigerøret utført. Dette ble gjort for alle de tre materialmodellene, og kreftene og krumningen langs stigerøret ble lagret. Dette ble brukt som input til en detaljert, lokal modell som kunne regne ut spenningene i hver stålvaier langs tverrsnittet. Basert på spenningshistorien ble det gikk et utmattingsestimat. Responsen til stigerøret for bølger i planet og i 45 grader ble undersøkt, samt en irregulær sjøtilstand.

Den ikke-lineære modellen anslo en årlig skade som var 25% høyere enn den lineære modellen som antok at lagene ikke kunne slippe. Den lineære slipp-modellen, som er mest lik dagens praksis, estimerte en skade som var 7 ganger høyere enn den ikke-lineære modellen. Denne lineære modellen ga et veldig konservativt estimat på den dynamiske responsen og utmattingsskaden. Når det kom til tidsforbruket, så brukte den ikke-lineære modellen omtrent tre ganger lenger tid. Ved å bruke en dedikert analysemaskin burde en full irregulær analyse være ferdig i løpet av fire dager.

Den økte bevegelsen av skipet når bølgene hadde en retning på 45 grader førte til tidligere slipp mellom lagene. Dette førte til en litt større forskjell mellom den

ikke-lineære og den lineære slipp-modellen. Den ikke-lineære effekten virker å være mer kritisk når det er bevegelse i og om alle akser.

Disse resultatene viste at man ved å inkludere den ikke-lineære effekten kan redusere estimatet av utmattingsskaden betraktelig, sammenlignet med å bruke den over-konservative lineære slipp-stivhet modellen. Dette kan bli brukt for å vise at design, som ville blitt forkastet ved å bruke en lineær modell, kan være trygge med tanke på utmatting. Dette åpner opp for mer økonomiske løsninger, uten at det går på bekostning av sikkerheten. Ytelsen til dagens maskiner er god nok til at det er realistisk å inkludere denne ikke-lineære effekten.

Contents

List of Figures

List of Tables

Nomenclature

Abbreviations

ASD	Allowable Stress Design
FEM	Finite Element Method
LRFD	Load and Resistance Factor Design
MM	Moment Model
RAO	Response Amplitude Operator
SBM	Sandwich Beam Model
TDP	Touch Down Point

Greek letters

α	Lay angle of tendon [deg]
α_1	Mass proportional term in Rayleigh damping [-]
α_2	Stiffness proportional term in Rayleigh damping [-]
$\Delta\sigma$	Stress range [MPa]
κ_f	Full slip curvature [1/m]
μ	Frictional coefficient [-]
ϕ	Circumferential coordinate of pipe cross section [rad]
Π	Potential energy [J]
τ_p	Pipe torsion [rad/m]
τ_t	Shear force per unit length [N/m]

ε_p Overall pipe strain [-]

Indices

ext External

ij Indicates the force in i-direction due to displacements in j-direction

int Internal

j Tensile layer number j

i Tendon number i

Roman letters

ΔK Stress intensity range [MPa $m^{0.5}$]

A Area of pipe [m^2]

A_t Cross section area of tendon [m^2]

b Breadth of tendon [m]

C_A Added mass coefficient [-]

C_D Drag coefficient [-]

E Elastic modulus [Pa]

EA Axial stiffness [N]

EI Bending stiffness [Nm^2]

F_f Fill factor of layer [-]

G Shear modulus [Pa]

GI_T Torsional stiffness [Nm^2]

k Shear stiffness factor [-]

M_c Bending moment at which layers start to slip [Nm]

M_f Bending moment at which layers are at full slip [Nm]

N Number of tensile layers [-]

N_c Cycles until failure with mean stress taken into account

N_i	Number of cycles
P	Pressure [Pa]
q_r	Radial line load [N]
R	R-ratio describing stress range [-]
R_j	Mean radius of layer [m]
S_a	Alternating stress [Pa]
S_c	Corrected stress [Pa]
S_m	Mean stress [Pa]
S_{max}	Max stress [Pa]
S_{min}	Min stress [Pa]
S_{uts}	Ultimate strength [Pa]
T_e	Effective pipe wall tension [N]
T_w	True pipe wall tension [N]
t_{tot}	Total thickness of tensile layers [m]
u	Displacement [m]
v_p	Tendon displacement [m]
v_s	Longitudinal displacement [m]
a	Constant in the SN-curve determined by experiments
m	Constant in the SN-curve determined by experiments
N	Number of cycles

Chapter 1

Introduction

The flexible riser is made up of a number of different layers each serving a specific purpose. These layers consist of both polymer sheaths and steel layers, including tensile armouring steel tendons. Due to internal pressure and tension in the pipe, these layers will stick to each other as long as bending moment is below a certain limit. When this limit is exceeded, these layers will slip. This stick-slip effect results in the distinctive non-linear response a flexible riser has. One bending cycle may thus result in an hysteresis loop.

Taking this effect into account will require more computational power, and the analyses will take longer. Hence, current practice consists of assuming the global behaviour of the flexible riser to be linear. The stiffness of the riser is given the same value as if the riser was depressurised, resulting in a much lower stiffness than in real life. This leads to an over-estimate of the response and the fatigue damage in the riser, and the design not being as efficient as what it could be.

In the recent years, the computational power has significantly increased, and this in combination with improved pipe models may now be able to open up for the use of a non-linear constitutive model to account for the real behaviour of a flexible riser. The purpose of this thesis is to investigate on the use of a model taking the stick-slip effect into account, and how it differs from the current practice. The performance of this non-linear model, both regarding the dynamic response and improved accuracy of the fatigue damage estimate, is of interest.

Three different constitutive models will be investigated, consisting of two linear models and one non-linear model. The first linear model will be given the same stiffness as if the pipe layers were stuck and the second linear model will be given the same stiffness as if the pipe was depressurised, which is most commonly used today. The non-linear constitutive model will take the stick-slip effect into account, and will hence be the most realistic model.

These models will be investigated by using the following method: A global analysis

will be performed for each of the models, where the main output will be the tension and curvature variation. This history will be input to a state of the art computer program to calculate the stresses on a local level. From these stress series, the fatigue damage can be estimated for each model.

To see if this analysis method is a realistic option in today's fatigue calculations of flexible risers, the time consumption using the non-linear model is of interest. In addition, the difference in the results obtained by using the linear models and by using the non-linear model is important. This non-conservative approach utilising the real behaviour may be able to demonstrate a safe design taking into account even more challenging loads, along with realistic pipe annulus environments.

Chapter 2

Flexible Risers

2.1 General

In the early 1960's, the French Petroleum Institute (IFP) started working on unbonded flexible risers, partly funded by the French taxpayers. Over a decade later, a patent for an unbonded flexible pipes was a reality. The unique characteristic of this pipe was its composition of both polymer sheaths and steel layers. This resulted in a pipe having the desired flex and at the same time the strength to be able to withstand large dynamic movements resulting from harsh environmental loads [PSA, 2013].

It was quickly discovered that the behaviour of the flexible pipe could be used in a broad range of applications. As a response to this, the Royal Norwegian Council for Scientific and Technical Research started a three-year research program in the period between 1989 and 1991. The overall goal was to make sure that the flexible pipes had a standard conforming to the environment at the Norwegian continental shelf. The final report became an initial guideline for safe design of flexible risers [Berge et al., 1992].

The flexibility of the riser has given it several advantages. Storage and installation is simpler, and the possibility of a permanent installation between the vessel/platform and the seabed template are two important reasons. A flexible riser is not subjected to vortex induced vibrations, which rigid risers can be, due to its high damping factor.

The flexible pipes are divided into bonded and unbonded flexible pipes. The focus in this thesis is on unbonded flexible risers, so terminology as unbonded flexible pipes and flexible pipes are here equivalent. The same applies for pipe and riser. A flexible riser is also a flexible pipe, but this is not necessarily valid the other way around.

2.2 Pipe layers

Flexible pipes are made up of several different layers, each with a specific purpose. Depending on the reservoir pressure and water depth, the flexible riser will need to resist high internal and external pressure. The global movements that the riser is being subjected to can lead to high bending moments, tension and torsion loads. Each layer is specifically designed so that combined; the riser can withstand all of these forces.

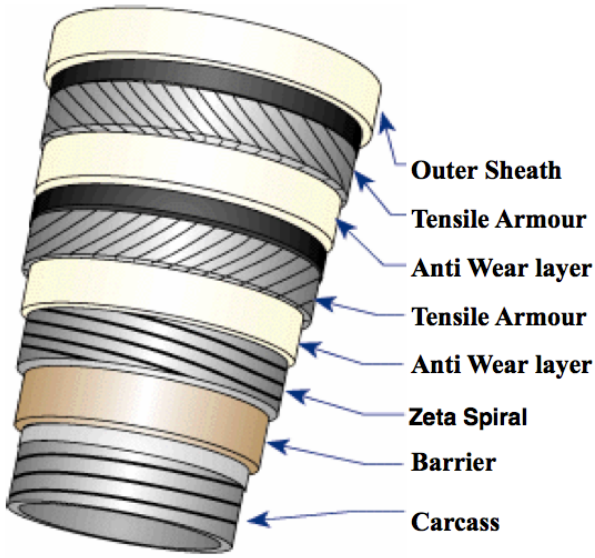

Figure 2.1: Flexible pipe layers [Tan et al., 2007].

Figure 2.1 shows the composition of a typical flexible pipe. The main layers and their function are as following [Berge et al., 1992]:

- **Steel carcass**: This layer has a corrugated structure, and can therefore only provide support for the external pressure. It also prevents the internal thermoplastic layer from collapsing in case of a sudden pressure drop.
- **Internal thermoplastic barrier**: This layer is meant to seal the transported fluid.
- **Zeta spiral**: The purpose of the zeta layer is to provide resistance against the internal pressure. It consists of Z-shaped wires made of steel so that wear due to interference with the thermoplastic sheath is minimal. This layer can also resist some external pressure.
- **Anti wear layer**: This layer reduces the friction between the zeta spiral and the tensile layers, thus leading to less wear.

- **Tensile layers**: This armour provides resistance for the axial forces, the bending moment and the torsional moment. It consists of two layers of flat steel wires with opposing lay angles. It is common to use anti-wear tape (and/or lubrication) to reduce friction, and hence wear, between these two layers. The lay angle is typically between 20 and 60 degrees [Sævik, 2013].
- **External thermoplastic sheath**: The purpose of this layer is to provide sealing against the external fluid. This is important as failure in this layer can lead to corrosion in the steel layers, leading to a greatly reduced fatigue life.

2.3 Configurations

There are several different ways to connect the flexible riser to the seafloor. Figure 2.2 shows the main configurations being used today. The difference lays in how buoyancy modules are being used and how they are being anchored. The existing seabed layout may limit which configuration that could be used.

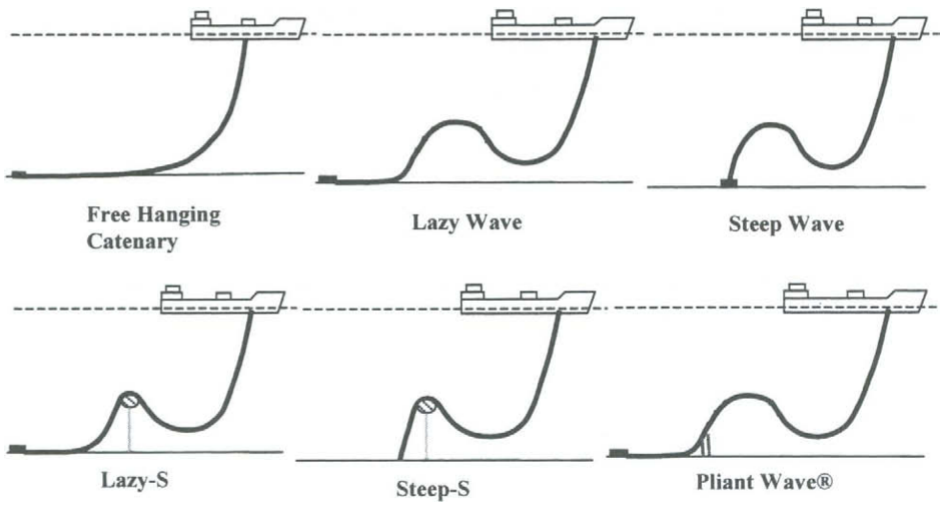

Figure 2.2: An overview of the main flexible configurations [Bai and Bai, 2005]

The governing factors that decides which configuration to be used is mainly the water depth, environment and vessel motions, hang-off locations and the numbers risers. Some of the configurations results in less movement of the risers, and others can reduce the top tension if the weight capacity of the vessel is critical. A brief summary of the configurations is given below [Bai and Bai, 2005]:

- **Catenary:** In this configuration, the riser is hanging freely down to the touch down point (TDP) and on to the seabed. It is anchored away from the

TDP, and the subsea structure required is simple, typically just an anchor. Depending on the water depth, the top tension can be high in this configuration. The vessel movement is directly transferred to the whole riser, so it should have sufficient resistance against buckling and birdcaging at the TDP.

- **Lazy Wave:** This configuration differs from the catenary with the buoyancy modules that has been clamped on to the riser. This results in less tension, but the main advantage is that the vessel movements are not being transferred to the TDP. The riser is anchored to the seabed away from the touch down point.
- **Steep Wave:** Similar to the lazy wave configuration, but instead of laying freely on the seabed, it is fixed to a subsea base and with a subsea bend stiffener. Hence, it has no movements on the seabed, which the lazy wave may experience.
- **Lazy S:** Compared to the above configurations, this is more expensive as it introduces a mid-water arch, which in turn is connected to the seabed with tethers. The global movements of the riser will be reduced, and movements at the TDP can be neglected.
- **Steep S:** It has some of the same advantages and disadvantages as the lazy S, but it is connected to the seabed with a subsea structure and a subsea bend stiffener. Both S-configurations will introduce a more complex hydrodynamic movement due to the inertia of the subsea buoy.
- **Pliant Wave:** This configuration is similar with the steep wave configuration, but the difference lays in that it is anchored in the TDP and the riser continues to the well. The disadvantage is that the subsea installation can be complex and expensive.

Flexible risers may also have a vessel-vessel or a vessel-platform connection, as shown in Figure 2.3. The computational analyses done in this thesis is of a jumper connected to a rigid platform. The length of the jumper must be chosen so that it is long enough to be fully submerged under all environmental conditions and with a sufficient weight to provide adequate tension at all times, and at the same time short enough to have a reasonable cost.

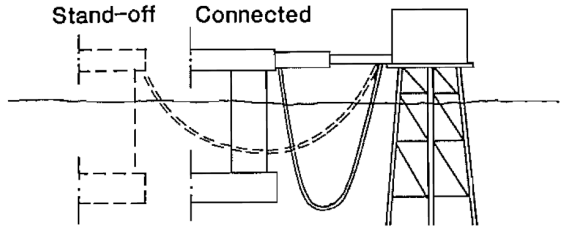

Figure 2.3: Jumper configuration [Berge et al., 1992]

2.4 Bending stiffeners

Bending stiffeners are typically applied at the riser top end, where it is rigidly connected to the vessel or platform. The idea is to provide a gradual transition between the rigid connection and the flexible pipe, so that excessive curvature and hence large bending stress is avoided. The two main types used on unbonded flexible risers are bend stiffeners and guiding funnels (like the bell mouth). The difference lays in that bend stiffeners uses an elastic-plastic material to provide an additional stiffness, while the guiding funnels provides a fixed support allowing no further bending of the riser.

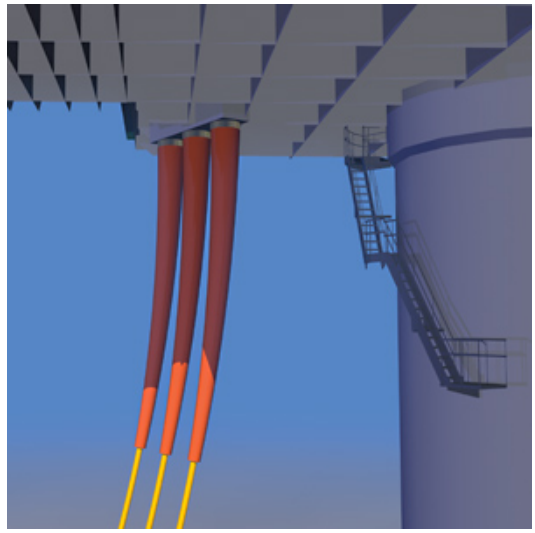

Figure 2.4: Shows bend stiffeners attached to the riser top end [BMP, 2014]

Design of the bend stiffener can be challenging, as the final design is dependent on whether it is being designed to be optimal with regard to extreme loads, or long fatigue life. For most cases, the extreme load will be the governing design factor. The basic idea behind bend stiffener design is that the pipe should have a constant curvature for a given load. Figure 2.4 shows the geometry and location of the bend stiffeners.

There are typically two critical points in the bend stiffener, where the curvature limit may be exceeded. This is at the tip of the bend stiffener and at the rigid connection. The final design of a bend stiffener is a result of an iteration process, as the loads acting on bend stiffener area of the riser is a function of the bend stiffener's length and stiffness. In addition, it needs to fulfil the requirements for a safe design both with respect to the extreme loads and the fatigue damage.

2.5 Design codes

There are two main design code sets that exists today. The design codes provided by Det Norske Veritas (DNV GL) and the design codes provided by the American Petroleum Institute (API). The standard provided by International Organization of Standardization (ISO) is identical to API's standard.

2.5.1 Det Norske Veritas

DNV is basing their standards on the Load and Resistance Factor Design (LRFD) design principle, which means that both the loads and the resistance are scaled with a statistically determined load factor [DNV, 2012]. This can be expressed as

$$S_d(S_P; \gamma_F \cdot S_F; \gamma_E \cdot S_E; \gamma_A \cdot S_A;) \leq \frac{R_k}{\gamma_{SC} \cdot \gamma_m \cdot \gamma_c} \tag{2.1}$$

where Sd denotes design load, γ is a load factor, F, E and A stands for functional, environmental and accidental load, respectively. On the right side, R_k is the resistance, and γ_{SC} is a resistance factor dependent on the class, γ_m is a material resistance factor and γ_c is a resistance factor to account for special conditions.

The load factors on the left side take account for uncertainties and incomplete knowledge of the external loads, and the resistance factors takes account for variability in strength and uncertainties of the resistance model.

The main design codes regarding flexible risers, and relevant for this thesis is:

- **DNV-OS-F201 Dynamic Risers**, containing information about design criteria, requirements and the structural design and analyses of flexible risers, both for static and dynamic loading [DNV, 2010a].
- **DNV-RP-F204 Riser Fatigue**, outlining the methods for performing fatigue calculations on flexible risers. These recommendations are based on fatigue tests and fracture mechanics [DNV, 2010b].

In addition, DNV-RP-C205 contains information about predictions, modelling and analyses of environmental loads (wind, wave and current). DNV-RP-F203 contains design criteria related to riser interference. DNV-RP-F206 contains suggestion about how to ensure that the riser system is run cost effectively, reliable and safely, and DNV-RP-F101 contains recommendations regarding concept development, design, construction and decommissioning of pipeline systems.

2.5.2 American Petroleum Institute

API is using the Allowable Stress Design (ASD) method, which are much simpler than the LRFD method used by DNV. This method expresses the allowable stress

as a safety factor multiplied with the yield stress, as shown in Equation (2.2). The weak side with ASD is that stress is not necessary a good measure of resistance, and it does not take into account the variation of neither the load nor the resistance.

$$\sigma = n \cdot \sigma_y \tag{2.2}$$

σ is the allowable stress, which is a safety factor (n) multiplied with the yield stress (σ_y).

The two relevant standards written by API covering flexible risers are

- **API 17J Specification for Unbonded Flexible Pipe**: Covering functional requirements, design requirements and requirements regarding to material choice and manufacturing. In addition, minimum requirements for testing are specified [API, 2008].
- **API RP 17B Recommended Practice for Flexible Pipe:** This standard provides guidelines for design, analysis, manufacture, testing, installation and operation of flexible pipes [API, 2002]

2.6 Failure of flexible risers

To ensure safe design of flexible risers, it is important to understand some basic factors that could lead to premature failure. It is normally distinguished between the failure drivers, which speeds up the failure process, and the failure modes, which describes how a riser can fail. According to API [2008], over 40 different failure modes have been reported. All of these will naturally not be mentioned, but the most common failure modes from a structural point of view will be mentioned.

2.6.1 Failure drivers

The most important failure drivers as discussed in Bai and Bai [2005] is summarised below.

Temperature

Temperature is a failure driver that mostly affects the internal polymer sheath. Changes in temperature can lead to stress cycles, which in turn can lead to cracking or aging of the internal sheath. This can lead to leakage of the internal fluid into the steel layers.

Pressure

Excessive pressure can cause failure of the tensile layers. The pressure is however carefully monitored, and the probability for this to happen is therefore low. Pressure cycles can contribute to the fatigue damage of tensile layers. Damage to the external sheath can lead to leakage and pressure on the internal sheath.

Diffusion of gases through the internal sheath can lead to a pressure built-up in the annulus. This is critical if the riser does not have a carcass. During an emergency shut down, the rapid internal pressure drop can, combined with the pressure in the annulus, lead to a collapse of the internal sheath.

Fluid composition

The content of the transported fluid can also speed up the failure process. CO_2 and H_2O can cause pitting, hydrogen-induced cracking and sulphur stress cracking for both the carcass and the cross-wound armours by diffusing through the internal sheath. Seawater can over time diffuse through the external sheath and also be threatening to the tensile layers. Corrosion fatigue will be covered later in Section 5.8.

Internal erosion due to sand in the transported fluid can also be critical over time, especially where the riser curves.

External components

External components like buoyancy modules and bend stiffeners must be kept intact as they are protecting the riser. If these components fail, this can lead to rapid failure of the riser. Buoyancy for example, looses some of its buoyancy over time, which would result in a different configuration. This is normally accounted for with a safety factor.

2.6.2 Failure modes

These failure modes are in general related to service loads that the riser will be subject to during its lifetime. API [2002] has a comprehensive list of failure modes. Identification of the failure mode is critical, and according to DNV [2010a] these shall be identified and made sure no limit state is exceeded. A summary of the most important failure modes is given below, and for the design solution to avoid these problems, refer to API 17B.

Collapse and bursting

The carcass can collapse as a result of excessive tension or pressure. High loads during installation can lead to collapse or ovalisation of the carcass. If seawater leaks through the external sheath due to damage, this high hydrostatic pressure can cause collapse of the internal polymeric sheath. Excessive internal pressure can cause rupture of the pressure armours (including carcass) or the tensile armours

Tension and compressive failure

Excessive tension can cause rupture of the tendons, and collapse of the pressure armours or the internal sheath. Excessive compression can lead to birdcaging of the tensile armours or buckling of the pipe.

Over-bending and excessive torsion

Over-bending can lead to rupture or collapse of the internal sheath, collapse of the pressure armours or cracks in the external sheaths. Excessive torsion can lead to rupture or birdcaging of the tensile armour layers, and collapse of internal sheaths or carcass.

Fatigue

High number of cycles can lead to fatigue failure of the tensile armour layers or the pressure armour wires.

Erosion and corrosion

Erosion and corrosion can lead to failure of the carcass. Corrosion can lead to failure of the pressure and tensile layers due to contact with seawater or diffused gases.

Chapter 3

Mechanical Behaviour

The unbonded flexible riser consist of several different layers, as has been shown in Figure 2.1. The geometry of these layers and their interaction results in a complex behaviour. It is the tensile layers that take up the axial- and bending stresses. These layers are essential in the stick-slip effect, which is fundamental to understand in order to establish the constitutive models. An important part will therefore belong to the understanding why and when these layers slip, the corresponding bending moment needed and the stresses that results from this behaviour.

This chapter will present theory of the local behaviour of a flexible riser. It is not limited to, but includes, theory on what BFlex2010 and SIMLA is based on.

3.1 Orientation tendons

The tensile layers consist of a several flat steel wires, commonly referred to as tendons. The number of tendons is dependent on each layer, but is function of the radius of the layer and the desired fill factor. A typical fill factor for the tensile layers is 0.9 [Sævik, 2014].

These layers have opposite defined lay angles, α, and is even in number to ensure as little coupling between the axial and torsional behaviour. The relevant stresses in flexible pipe are those in the longitudinal direction of the tendon, and not along the pipe center line. The forces and orientation of the tendons relative to the local element coordinate system are defined in Figure 3.1.

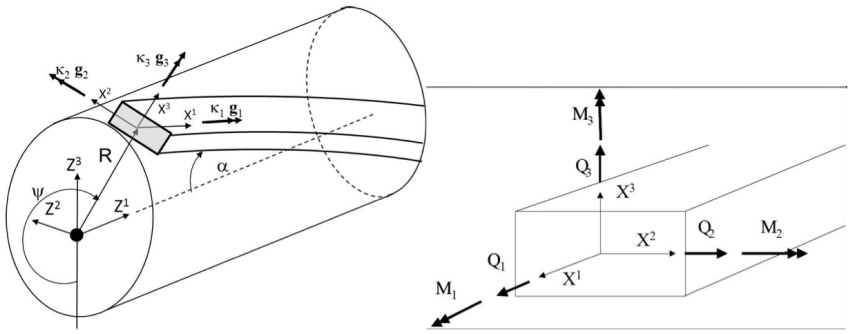

Figure 3.1: Tendon orientation and forces relative to the local element orientation [Sævik, 2013]

3.2 Behaviour in bending

3.2.1 General

The flexible riser has a complex behaviour when being subjected to a bending moment. The friction between the layers results in a distinctive, non-linear response. This section will explain the stick-slip effect, when the initial and full slip occurs, and the corresponding bending moment. Please note that Section 3.3 is devoted to the stresses and strains in the tendons.

If the bending of the flexible pipe could be described in the same way as a beam, the relationship between the applied moment and the curvature of the riser can be described as

$$M = EI\,\kappa \tag{3.1}$$

where M is the bending moment, EI is the stiffness in bending and κ is the curvature. The curvature is equal to one divided by the radius of the point it is being bend about, i.e. how much it curves. This relationship is linear, and would apply if the pipe was depressurised. However, this is not how the pipe behaves when it is pressurised, and there are contact forces between the layers. This will be explained in the following.

The frictional factor is an important parameter both when it comes to the global response of the pipe and the calculation of the stresses. Due to tension and pressure forces, there are contact forces on each layer. This leads to loads acting in the radial direction of a layer, and due to the friction between two layers, shear forces occur. These layers slip when the shear force is larger than shear capacity governed by friction. Slip of unbonded flexible risers have been studied in several articles, amongst them Kraincanic and Kebadze [2001] and Sævik [2011].

The two main longitudinal stress contributions from bending of pipes comes from the material stiffness and the stick-slip effect mentioned below. Prior to slip, the pipe behaves like a rigid pipe with a high stiffness. After slip, the material stiffness of the layers are the main contribution to the bending stiffness. The real behaviour in bending can be found as a sum of these to characteristics. For a flexible pipe consisting of two layers, the following figure shows how this works.

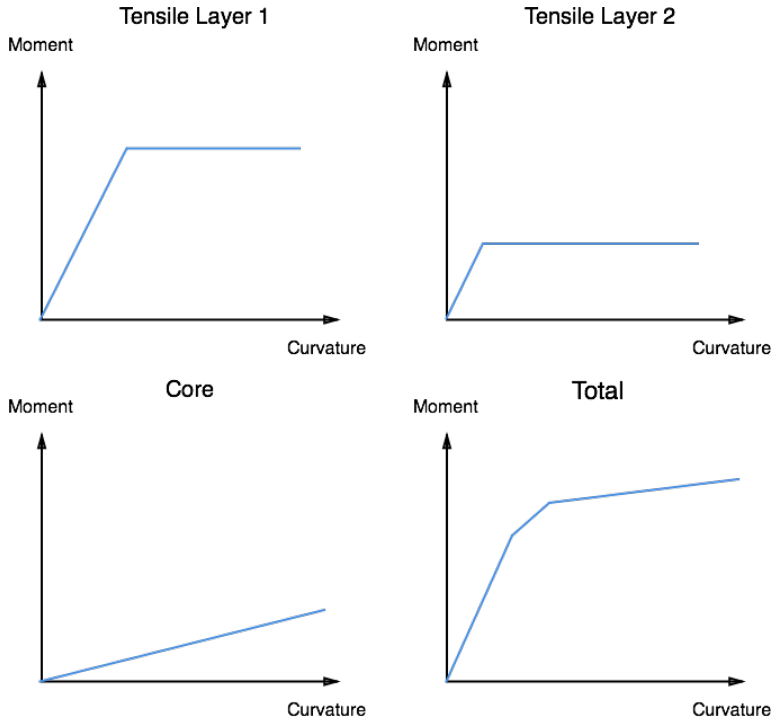

Figure 3.2: Contribution of each layer to the total bending stiffness

An interesting behaviour is that the inner tensile layer slips at a three times larger moment than the outer tensile layer. This is when there are two tensile layers, and can be explained by equilibrium considerations: Both layers are acting on the inner pressure liner with a normal force N, added together the reaction force becomes $2N$. In addition to experiencing this force, the inner tensile layer acts with its own normal force, resulting in a total frictional force of $3\mu N$.

3.2.2 Slip initiation

A pipe exposed to a bending moment will get a corresponding curvature according to Equation (3.1). For small curvatures, the pipe will behave like a rigid pipe, meaning that Navier's hypothesis is valid (plane surfaces remain plane). When

the shear stress between the innermost tensile layers exceeds the shear capacity governed by friction, the layer starts to slip. The corresponding curvature is defined as κ_c. The two main factors to consider when formulating a constitutive relation to model friction is a friction surface and a slip rule. By assuming a parabolic surface, and that the slip can be divided into an elastic and a plastic part, a material frictional law can be established. The reader should refer to Sævik [2010] for the derivation.

The shear forces on the tendons at the bending neutral axis will exceed the frictional capacity first, so this is where slip will initiate. This means that the whole cross section does not slip at the same time. When the pipe is bend further, the slip will progressively move along the cross section until it reaches the point with maximum compression/tension. This can be seen in Figure 3.3 below.

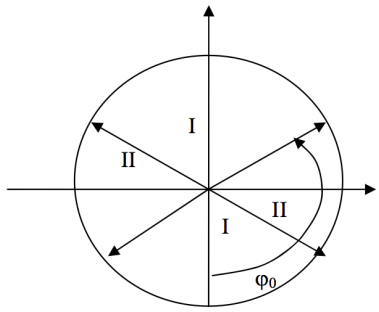

Figure 3.3: Definition of slip regions, with slip happening in region II [Sævik, 2010].

To be able to determine the moment and curvature at which the pipe starts to slip, an analytical expression can be derived. In the following, bending about one axis is assumed.

The forces in each tendon before slip can according to Sævik [2010] be described as:

$$S = -EA\cos^2\alpha\, R\cos\phi\,\kappa \tag{3.2}$$

where EA is the axial stiffness consisting of the tendons E-modulus and area, α is the lay angle, ϕ is a circumferential coordinate starting at the compressive side of the pipe and κ is the curvature about the bending-axis.

The bending moment needed to reach slip and full slip can now be derived based on Equation (3.2.2). The shear force, τ_t, per unit length of the tendon can be found by differentiating the expression for force in a tendon with respect to the length s:

$$\tau_t = EA\cos^2\alpha\sin\alpha\sin\phi\,\kappa \tag{3.3}$$

The maximum shear capacity, τ_c, for bending about the y-axis, can then be expressed as the maximum line load multiplied with the frictional coefficient, μ:

$$\tau_c = \mu(q_r^i + q_r^{i+1}) \tag{3.4}$$

The critical curvature is defined at the point where the shear force in the tendon equals the shear capacity, which can be found be setting the two above equations equal to each other. This gives an expression for the critical curvature at which slips initiates, κ_c:

$$\kappa_c = \frac{\mu(q_r^i + q_r^{i+1})}{EA\cos^2\alpha\sin\alpha} \tag{3.5}$$

By utilising symmetry, thin shell theory and integrating up the stress, the corresponding bending moment at which slip occurs can according to Sævik [2011] be found as

$$M_c = \frac{\mu(q_r^i + q_r^{i+1})R^2\cos\alpha\ n}{2\sin\alpha} \tag{3.6}$$

3.2.3 Full slip

There is a transition between slip initiation and full slip. This is shown in Figure 3.5. Based on the same principles as the equations above, the relationship between the curvature and the minimum slip curvature can according to Kraincanic and Kebadze [2001] be found to be

$$\kappa_f = \frac{\pi}{2}\kappa_c \tag{3.7}$$

where the f index notes full slip. An example of how the critical curvature varies along the cross section can now be seen in Figure 3.4. The cross section behaves symmetrical about the neutral axis.

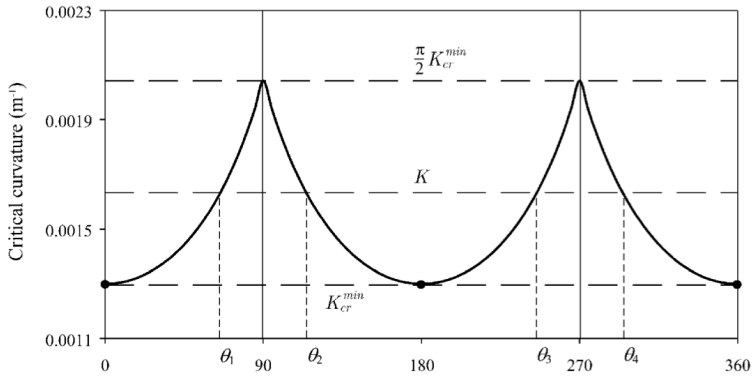

Figure 3.4: Critical curvature variation along the cross section. Note that θ starts at the bending neutral axis. [Kraincanic and Kebadze, 2001]

A similar relationship is derived by Kraincanic and Kebadze [2001] for the relationship between the minimum slip bending moment and full slip bending moment:

$$M_f = \frac{4}{\pi} M_c \tag{3.8}$$

The response of an unbonded flexible riser can now be graphically explained as in Figure 3.5.

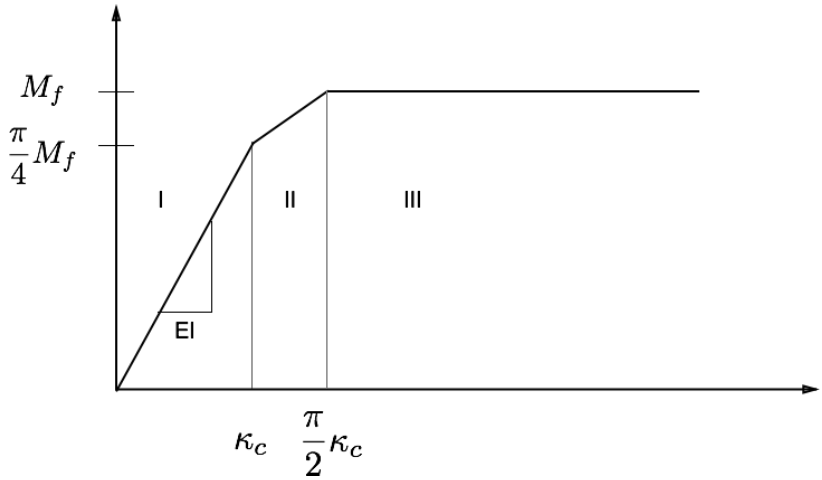

Figure 3.5: A characteristic moment curvature diagram, where I is the stick region, II is slip of parts of cross section and III is full slip.

If the riser is in the stick-regime, i.e. below the critical curvature, the bending stiffness can be expressed as

$$EI = EI_e + \sum_{i=1}^{N} F_{f_i} \cos^4 \alpha_i \, \pi \, R_i^3 \, t_i \tag{3.9}$$

Here EI_e is the stiffness contribution from the elastic behaviour of the layers and N is the total number of tensile layers. If the curvature is above the full slip curvature, the second term in this equation vanishes.

3.3 Stresses and strains

A general element of the pipe can be seen in Figure 3.6, along with how the stress is defined in the element. Stresses in the element are a result of axial forces, bending moments and torque. The axial force is a result of the weight of the riser, along with the vessel motions. Bending and torsion moments are result of installation and environmental loads. The main stresses occurring in a flexible pipe is, according to Sævik [2013] the three normal stresses σ_{11}, σ_{22} and σ_{33}, along with the shear stresses σ_{12}, σ_{23} and σ_{13}.

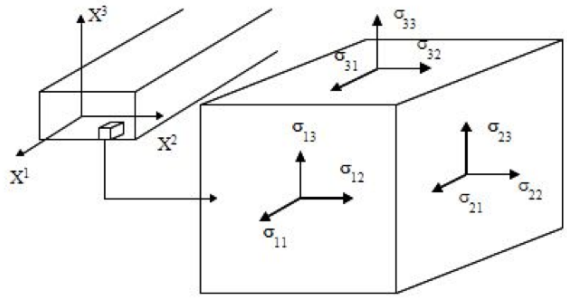

Figure 3.6: Stress definitions in an general infinitesimal element [Sævik, 2013]

The environmental loads are generally designed to be taken up by the steel layers, as these are much more resistant to higher stress levels. As explained in Section 2.2, these layers are the carcass, the zeta-spiral and the tensile layers. The carcass' main function is to resist external pressure, and does not take up much longitudinal stress. The zeta-spiral is both providing support for the polymeric sheaths and resisting internal pressure, which in most cases leaves the largest stress variation to happen in the tensile layers. These tensile layers are made up of several steel tendons having a predefined lay angle, and are oriented along a helical path along the pipe. The relationship between the stresses in the pipe's longitudinal direction and the tendons longitudinal direction will be of a factor $\sec \alpha$ higher in the tendon.

Fatigue could be of interest in both tensile layers and pressure layers, but in most cases, the tensile layers will experience the largest stress variation. As long as the

pipe is moderately pressurised, the zeta layer will not be a problem with respect to fatigue. Due to the nature of this thesis with focus on the fatigue in the tensile armours, this section will therefore be devoted to explaining how the global loads are affect the stresses in the tendons. To have a clear and unison definition of the forces and tendon directions, see Figure 3.1.

The area taken up by the tendons are described by a fill factor, F_f, which is convenient to use when calculating the stress each wire has to take up in the longitudinal direction. Mathematically, this is described as

$$F_{f_j} = \frac{n_j b}{2\pi R_j \cos\alpha} \tag{3.10}$$

where the subscript j denotes a property for layer j, n_j is the number of tendons in this layer, b is the tendon breadth, R_j is the mean radius and α the lay angle.

3.3.1 Due to axial loading

The main factors resulting in stresses due to axial loading is gravity, buoyancy, internal pressure and external pressure. The tensile layers will take nearly all of the axial force, and by considering axial equilibrium of the stresses in the tendons and the external loads, the equation becomes

$$\sum_{j}^{N} n_j \; \sigma_{11_j} \; A_t \cos\alpha_j = T_w = T_e + P_i \; \pi r_i^2 - P_e \; \pi \; r_e^2 \tag{3.11}$$

Where on the left side, N is the total number of layers, σ_{11} the axial stress in the tendons in layer j and A_t is the cross section area of a tendon. On the right side, T_w is the true pipe wall tension, T_e is the effective tension, P is the pressure and r the radius. int denotes internal and ext denotes external.

By manipulating Equation (3.11) and assuming equal lay angle and fill factors for the layers, the following expression could be used to estimate the stresses in the tensile layers due to axial loading.

$$\sigma_{11} = \frac{T_w}{2\pi R \; t_{tot} F_f \cos^2\alpha} \tag{3.12}$$

Here, t_{tot} is the total thickness of the tensile layers and R is the mean radius of both tensile layers.

By using standard beam formulation for the axial strain in a tendon, the axial strain can according to Sævik [2013] be expressed as

$$\varepsilon_{11} = \cos^2\alpha\,\varepsilon_p + \frac{\sin^2\alpha}{R}\,u_3 + R\sin\alpha\cos\alpha\,\tau_p \tag{3.13}$$

where ε_p is the overall pipe strain and τ_p is the pipe torsion along the x-axis.

By using the stress strain relationship and combining Equation (3.12) and (3.13), the axial stiffness of the pipe in axial direction can be expressed as

$$EA = 2\pi R\,t_{tot}F_f E\cos^2\alpha(\cos^2\alpha - v_a\sin^2\alpha) \tag{3.14}$$

here, v_a is being introduced, which is the apparent Poisson's ratio defined as the axial strain versus radial contraction.

3.3.2 Due to torsion

When the pipe is being subject to a torsional moment, M_T, the corresponding stresses can also be found by considering equilibrium. The axial stresses due to torsion can then be written as

$$\sigma_t = \frac{M_T}{nA_tR\sin\alpha} \tag{3.15}$$

By combining Equation (3.13) and Equation (3.15), the torsional stiffness of the riser can be estimated as

$$GI_T = nEA_tR^2\sin^2\alpha\cos\alpha \tag{3.16}$$

Since the tensile layers have a different mean radius, and the fill factor should approximately 0.9 for each layer, the number of tendons will increase in each layer. This leads to a slightly unsymmetrical behaviour in torsion.

3.3.3 Due to bending

The behaviour of a flexible pipe subjected to bending, and the associated curvatures and bending moments have been explained in Section 3.2. This section is further devoted to describing the stresses that occur along the cross section during bending.

The longitudinal stress contribution due to friction between layers can be found by considering the shear force acting on the tendon. This can be found by multiplying the line load with the length over which this load acts, with the frictional factor divided by the tendon area:

$$\sigma_{11} = \frac{\mu(q_r^i + q_r^{i+1})}{A_t} \cdot \frac{R\,\varphi}{\sin\alpha} \tag{3.17}$$

Here, φ is an angular coordinate defined according to Figure 3.3, illustrating how much of the cross sectional area that has slipped. q_r^i is the radial line load on layer i and μ is the frictional factor. The stress above is only valid in the region that has slipped. The second term is the length over which the line load acts, and is found by geometric considerations of a tendon.

For the region still in the stick-regime (region I in Figure 3.3), the longitudinal stress can according to Sævik [2013] be expressed as

$$\sigma_{11}(\varphi) = E\cos^2\alpha\; R\;\kappa_f\;(\sin\varphi - \sin\varphi_0) + \frac{\mu(q_r^i + q_r^{i+1})}{A_t} \cdot \frac{R\varphi}{\sin\alpha} \tag{3.18}$$

As can be seen in Figure 3.3, a relationship between the minimum slip curvature (κ_c) and the full slip curvature (κ_f) can be expressed as

$$\varphi_0 = \cos^{-1}\frac{\kappa_f}{\kappa_c} \tag{3.19}$$

Noting that full slip happens when $\varphi = \frac{\pi}{2}$, the stress at full slip can be expressed as

$$\sigma_{11} = \frac{\mu(q_r^i + q_r^{i+1})}{A} \cdot \frac{R\pi}{2\sin\alpha} \tag{3.20}$$

The total stress the tendon experiences; will be the sum of the stress due to axial, torsional and bending loads.

3.3.4 The Green strain tensor

The Green strain tensor is a way of measuring the deformation in the elements. This expression is based on an Euler-Bernoulli beam, which is the classic beam theory assuming that Navier's hypothesis is valid. In BFlex2010 , the second order term of the Green strain tensor is neglected, along with the coupling between axial strain and torsion, and shear deformations [Sævik, 2010]. This is a decent assumption as long as the strains are small and for thin elements.

The displacement in x-, y- and z-direction in the pipe elements may be written as

$$u_x = u_{x_0} - y\;u_{y_{0,x}} - z\;u_{z_{0,x}} \tag{3.21}$$
$$u_y = u_{y_0} - z\;\theta_x \tag{3.22}$$
$$u_z = u_{z_0} + y\;\theta_x \tag{3.23}$$

where u notes displacement, the subscripts x, y and z indicates along which axis, and 0 is referring to the initial position. The sub subscript x indicates the derivative in this direction.

The Green strain tensor can then be written as [Sævik, 2010]:

$$E_{xx0} = u_{x0,x} - y\ u_{y0,xx} - z\ u_{z0,xx} + \frac{1}{2}(u_{y0,x}^2 + u_{z0,x}^2) \tag{3.24}$$

Once the strain in the elements is known, Equation (3.13) can be used to find the tendon strain. The full derivation of the tendon strains can be found in Sævik [1992].

3.3.5 Constitutive relation for tendons

By assuming that the material is isotropic and behaves elastically according to Hooke's law, the constitutive relation for the tendons can be expressed as [Sævik, 1992]:

$$\sigma^{11} = E\ \varepsilon_{11} \tag{3.25}$$
$$\sigma^{13} = 2\ G_\tau\ \varepsilon_{13} \tag{3.26}$$
$$\sigma^{12} = 2\ G_\tau\ \varepsilon_{12} \tag{3.27}$$

where σ_{11} is the stress in axial direction, σ^{13} and σ^{12} is the shear stress in x-direction, due to displacement in y- and z-direction, respectively. E being Young's modulus of elasticity and G_τ being the shear modulus. ε denotes the strain, with the indices following the same logic as for the stresses.

3.4 Tensile armour models

There are different ways to model the tensile armours in BFlex2010 . Either by using the Sandwich Beam Model (SBM) or the Moment Model (MM). In both formulations, the transverse slip is neglected, which means that it follows a loxodromic path. This is illustrated in the figure below. During dynamic cycles, the transverse movement has shown to be small, which justifies this assumption [Sævik, 2010].

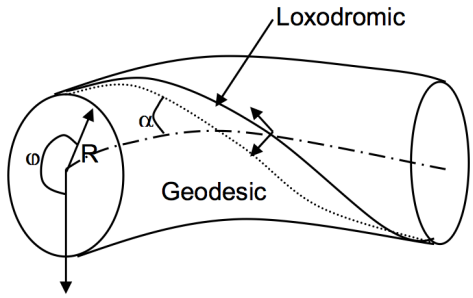

Figure 3.7: The tendons have a constant lay angle, ie it follows a loxodromic helical path [Sævik, 2010]

3.4.1 Sandwich beam model

In this model, the axial, torsional and bending stiffness is given for all layers except the tensile armour. These layers are then defined as a core, while the tendon armours are modelled separately. The stick-slip behaviour is then established as a shear stress versus relative deformation ratio for each of the layers. The equilibrium of each tendon due to shear interaction with the core layers is then considered. This way of modelling can be more computational demanding compared to the Moment Model, which is explained in the next section.

By using sandwich beam theory and defining the potential energy, Equation (3.28) can be established. The potential energy for each tendon would be the sum of the axial work done, the work done by bending the model and subtracting the external loads:

$$\Pi = \frac{1}{2}\int_0^l EA(\frac{\mathrm{d}v_s}{\mathrm{ds}})^2 + \frac{1}{2}k(v_s - v_p)^2\mathrm{ds} - Pv_p \tag{3.28}$$

where EA is the axial stiffness, v_s is the longitudinal displacement, v_p is the tendon displacement, k is a shear stiffness factor expressed as $\frac{Gb}{t_s}$, where G is the shear modulus, b is tendon breadth, t_s is thickness of virtual shear layer and P is the external load. By minimizing this equation, the equilibrium equation for a tendon can be found.

In BFlex2010 , ITCODE0 and ITCODE1 apply the SBM. The difference between these two iteration codes, is that the first calculates the slip from the inner layer and assigns this to all layers, while the second calculates the slip value for each layer.

3.4.2 Moment model

This model establishes the axial, torsional and bending stiffness for all layers except the tendons. The difference from the SBM is that a non-linear moment curvature relationship is established for each of the tensile layers. What is important in this model is the frictional interaction between the layers and the stick-slip properties. The stick-slip effect that this model is based on is presented in Section 3.2.

The advantage with the moment model is that it is easier to model, as it only models the tendons as tensile layers, while the SBM models each individual tendon. This simpler model also leads to a shorter computational time, as the stiffness matrix is less complex. The moment model may give less stress in extreme cases, but has proven to be similar to full scale test results with respect to fatigue [Sævik, 2011].

In BFlex2010 , ITCODE21 and ITCODE31 use the moment model. The difference is that the first calculates the moment curvature for the first layers, and assigns these properties to all layers, while the latter calculates the moment curvature graph for each layer.

3.5 Constitutive models

Three different constitutive models are being investigated in this thesis. The difference lays in which bending stiffness is used:

1. **Non-linear stiffness model**: The non-linear hysteresis effect is taken into account, resulting in the most realistic model.
2. **Linear stick-stiffness model**: The bending stiffness is given the same stiffness as if the layers are not allowed to slip.
3. **Linear slip-stiffness model**: The bending stiffness is given the same stiffness as if there is no friction.

The first model takes the stick-slip effect that arises when there are frictional forces between the layers, resulting in a non-linear response. This model is most similar to the real behaviour of a flexible pipe. The stiffness is quite high when the layers are in the stick region, but when the slip curvature is being exceeded the stiffness is significantly reduced. The material curve in bending allows for this to happen.

The last two models are both linear, but differ in which bending stiffness is being used. The second model uses the stick-stiffness, i.e. the stiffness when the curvature is below the slip curvature, and the tangential forces from the tendons are less than the max shear force governed by friction.

The last model uses the stiffness when full slip is assumed, which is significantly less than the previous model. This should lead to larger movements of the riser, which in turn leads to increased stresses and stress amplitudes. The result with respect

to both fatigue life and extreme loads will then be quite conservative. Using the slip stiffness in bending is current practice in the industry [Sævik, 2014].

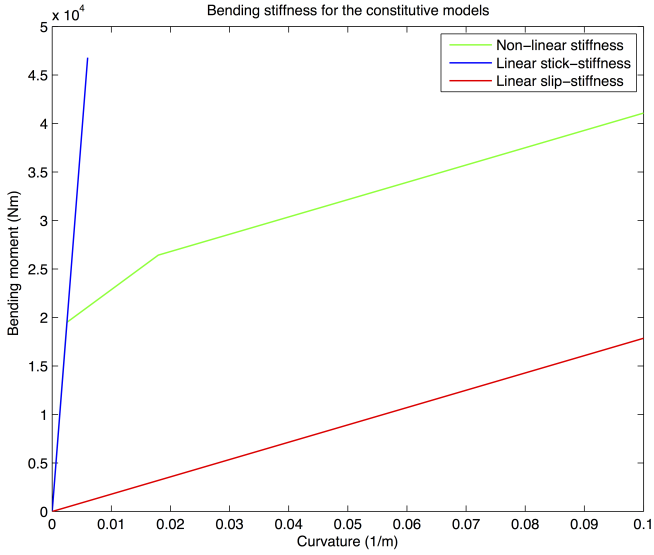

Figure 3.8: Comparison of the bending stiffness of the three constitutive models.

The three different models is plotted together in Figure 3.8. To avoid misunderstandings: The global model has been given the non-linear material model stated above. The riser is made up of polymeric sheaths and steel, and these materials will always behave linearly. However, the stick-slip effect will result in a non-linear behaviour, and this can be modelled by using an equivalent material that yields when the slip-curvature is exceeded. This does not affect the stresses, and neither the steel material nor the polymeric sheaths are yielding, but the fictive material is. This only results in the global response to be modelled correctly.

3.6 On hysteresis

The past practice with regard to the bending hysteresis has been to model the riser with linear bending properties. The response has then been extracted and used as input to in a more detailed local model. This has given a conservative estimate of the stresses and fatigue life. In the recent years, more resources has been used on the investigation of the hysteresis-effect. This section summarises the main findings and conclusions of these articles and identifies the current progress.

Tan et al. [2007] presented two models taking the non-linear hysteresis into account in 3D time domain simulations, developed by Orcina and Wellstream. The model developed by Orcina took the non-linear moment-curvature relationship into account be defining a bending vector. This vector consisted of the relationship between the bending moment and curvature for any given curvature increment. The global response can then be modelled correctly, but the stresses in the tensile wires remain unknown and have to be processed in a local model. This approach bears similarities with the approach in this thesis.

Wellstream developed a more sophisticated model, which was able to both output the three-dimensional bending response as well as stresses in each individual tensile wire. This is done by applying the bending moment resulting from environmental loads and calculating the corresponding curvature using the same model as above. Based on this curvature, the slip region at each time step is calculated, and this is used to determine the axial stress in each tensile wire. The bending moment contribution from each wire is then determined from the axial stress. This is again passed back to the global program (OrcaFlex), and used as input to calculate the curvature at the next time step.

The response of the riser was calibrated using actual test data. The conclusion of this study was that both models showed a very similar result on the bending moment vs curvature diagram, which is reasonable since the Wellstream model was using data based on the Orcina model. Implementing the hysteresis gave a significantly reduction in the curvature. The authors remarks that this is still an on-going process, and with the Wellstream model, they hope to be doing rainflow counting directly on the stress history from the global model, to be able to do accurate fatigue calculations.

Smith et al. [2007b] proposed new computational tools for dynamic analysis of flexible risers, considering bending hysteresis. They examined three different cases that would benefit from incorporating the bending hysteresis: Structural damping of cantilever beam due to frictional forces, seabed-riser interaction at TDP and response at hang-off of a shallow water steep-wave riser.

The results showed that the structural damping effect that arises from the frictional forces gives a significantly reduction in the movements. Incorporating the hysteresis effect is benefiting when examining extreme response of a riser at the touch down point, see Figure 3.9. The stick-slip effect would also lead to a large reduction in curvature variation at the critical points along the bend stiffener. They concluded that taking the hysteresis effect into account can allow for the use of lower cost solutions while still proving the design to be safe. In addition, it can open up for the use of solutions that would not be feasible with a conservative approach.

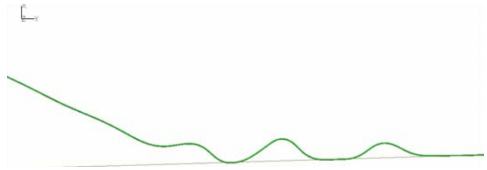

(a) Linear stiffness

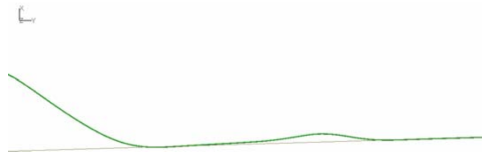

(b) Hysteresis

Figure 3.9: Extreme response at touch down with linear stiffness and hysteresis stiffness [Smith et al., 2007b]

[Smith et al., 2007c] have also performed fatigue analyses of flexible risers, taking irregular seas and hysteresis into account. Their approach was to model the hysteresis as several perfectly-plastic springs i parallel. The curvature and tension history were then extracted from the global model, and by processing this data through a local model, fatigue was calculated. This method is similar to the one used by Orcina. They concluded that implementing the bending hysteresis should be part of the analyses if a non-conservative estimate of the fatigue life needs to be performed.

Sævik [2011] presented two models that takes into account the stick-slip effect. These models are the moment model (MM), modelling the hysteresis with a non-linear moment-curvature diagram for each tensile layer, or the sandwich beam model (SBM), which takes into account the equilibrium for each tendon. These were further described in Section 3.4. Both models were tested against a full-scale model, were the MM was found to give the best fit for fatigue analysis.

The articles above found that taking the hysteresis effect into account is important, as it has two effects that reduce the bending motions. The first reason is that the stick-stiffness is significantly higher than the stiffness the pipe has when it is depressurised. For sufficiently small waves, the riser will behave linearly with a high stiffness, hence reducing the motions. The second is being related to the fact that frictional forces are always working against the movements. When flexible riser is being subjected to dynamic motion causing hysteresis, a hysteresis loop will be made. The area under this loop is proportional to the energy loss, due to frictional forces. Naturally, this has a damping effect on the global motions.

Chapter 4

Global Analysis

This chapter will present some of the basic theory on which the global analysis is based. The focus will lay on how the Finite Element Method (FEM) is implemented into SIMLA and BFlex.

4.1 Fundamental principles

The finite element method is based on three fundamental principles:

1. Material law
2. Equilibrium
3. Kinematic compatibility

The material law assigns a relationship between the stress and the strain of the material. Hooke's law or an elastic-plastic relationship between the stress and strain is normally applied.

All parts of the structure has to be in equilibrium. This can be mathematically described by using an energy variation, for example d'Alembert's principle of virtual work, which states that the sum of virtual work for all forces will be equal to the inertia forces.

Kinematic compatibility describes the relationship between strains and displacements. For beams, this principle requires that the strains can be expressed dependent of the nodal displacements or rotations.

4.2 Coordinate system

The Cartesian coordinate system is being used. The global coordinate system is earth fixed, where the x- and y-direction normally defines translation horizontally. The z-direction is used to describe depth. Thus, in 2D the y-axis is not being used. It is important to note that there is a local coordinate system associated with the riser elements in SIMLA. This coordinate system is always fixed to the riser, and can be seen in Figure 4.1. Here, the x-axis is along the element center line and the y-axis very often parallel to the global y-axis. The local z-axis can then be found using these two axes and the right hand rule.

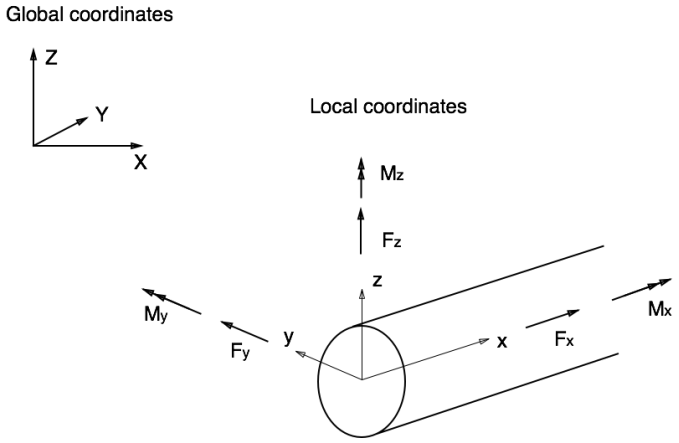

Figure 4.1: Local element orientation in the global coordinate system.

4.3 Morison's equation

The flexible riser is a slender structure. These structures are often characterised by a large wavelength - diameter ratio. This means that drag and viscous forces are the main contribution from the wave loads. Slender structures often have a circular cylindrical shape. The governing equation for calculation of wave loads on circular cylinders is Morison's Equation. This equation expresses the force dF on a very small part of the structure length, and can by using strip theory give the total force. The equation, taking into account the riser response, can according to Faltinsen [1990] be written as:

$$dF = \rho C_A \frac{\pi D^2}{4}(\dot{u} - \ddot{r})\mathrm{dz} + \rho \frac{\pi D^2}{4}\dot{u}\mathrm{dz} + \frac{1}{2}\rho C_D D\mathrm{dz}|u - \dot{r}|(u - \dot{r}) \tag{4.1}$$

where ρ is the density of the sea water, D is the diameter and dz is a strip of the cylinder. Dot stands for the time derivative. u is the velocity in x-direction of

the water particles, while r is the response of the cylinder. C_A is the added mass coefficient and C_D is the drag coefficient.

4.4 Equilibrium equation

The motion of a flexible riser undergoing large displacements can be derived by using the principle of virtual displacements and by demanding equilibrium. This leads to a non-linear second order differential equation, expressed as

$$\mathbf{M}\ddot{\mathbf{r}} + \mathbf{C}\dot{\mathbf{r}} + \mathbf{K}\mathbf{r} = \mathbf{R} \tag{4.2}$$

This is all on matrix form, where $\mathbf{M}$ is the mass matrix containing both the mass and the added mass, $\mathbf{C}$ is the damping matrix, $\mathbf{K}$ is the stiffness matrix and $\mathbf{R}$ is the load matrix. $\mathbf{r}$ is the displacement vector containing the riser elements, $\dot{\mathbf{r}}$ is the velocity vector and $\ddot{\mathbf{r}}$ is the acceleration vector.

Introducing Rayleigh damping can simplify the damping matrix. This method assumes that the damping matrix $\mathbf{C}$ can be written as a function of the mass and the stiffness matrix. This can be seen in Equation (4.3). By manipulating this equation, it is possible to choose the constants so that the desired damping level is met at a specified frequency. This frequency should normally be chosen to give a realistic damping at the dominating wave frequency. For structures undergoing large rigid body movements, the mass damping term (α_1) can be neglected. The damping matrix can then be set as a function of the stiffness matrix only, [DNV, 2010].

$$C = \alpha_1 \, \mathbf{M} + \alpha_2 \, \mathbf{K} \tag{4.3}$$

4.5 Geometrical description

The external loads may change the position in the Cartesian coordinate system of the elements studied, as well as the geometry of the element. There are three main formulations used to update the forces and stiffness matrix according to this change [Felippa and Haugen, 2005]. These are the Total Lagrange formulation, the Updated Lagrange formulation and the Co-rotational formulation. These formulations differ in how they are describing the change in geometry.

The Total Lagrange formulation refers to the initial configuration (C^0), and the Updated Lagrange refers to the last equilibrium position (C^n). The formulation used in BFlex and SIMLA is the Co-rotational formulation, and will be explained

further in the next section. The basic idea with all of these formulations is to separate the rigid motions of the elements from the local deformations.

4.5.1 Co-rotational formulation

The co-rotational formulation is based on the following definitions of the configurations: The initial configuration (C^0) serves as the standard reference point. Each element has attached a local coordinate system (C^R) that is allowed to translate and rotate freely with the element. The element deformation is described by a configuration C^D. An important assumption in this formulation, is that the strain has to be small, while displacements and rotations can be large [Felippa and Haugen, 2005].

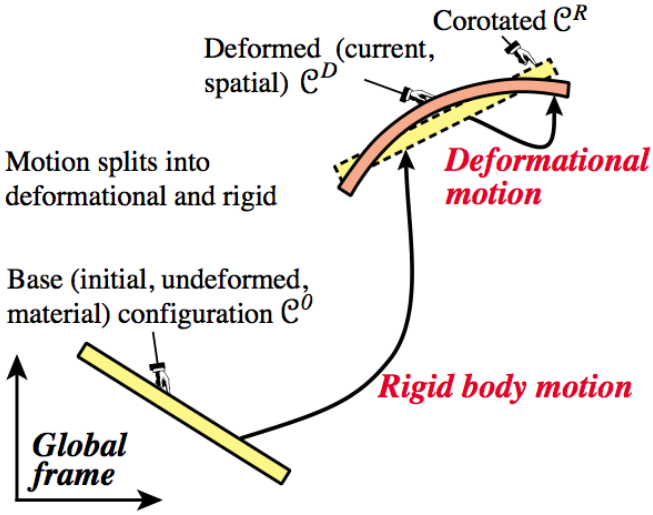

Figure 4.2: The element are allowed to translate and rotate, while the local coordinate system describes the deformation [Felippa and Haugen, 2005].

4.6 Non-linear behaviour

Flexible risers are subject to many different non-linear effects. For cases with small deformations and movements, all of these tend to be in the linear regime. The relationship between forces and displacement, stresses and strains can then be significantly simplified and still provide an accurate answer. As rotations and movements are becoming increasingly larger, the relationships becomes more complicated, resulting in more advanced mathematics being used. This increases the computational time.

Slender structures tend to undergo large rigid body motions, while the strains are being small. This typically leads to a non-linear geometric behaviour, while the material lies well within a linear relationship. The main non-linearity's are explained below.

4.6.1 Material

To understand how an increasing load is affecting the material, the relationship between the stresses and strains should be understood. This can be seen in Figure 4.3, and will now be further explained with basis in the stress-strain relationship figure.

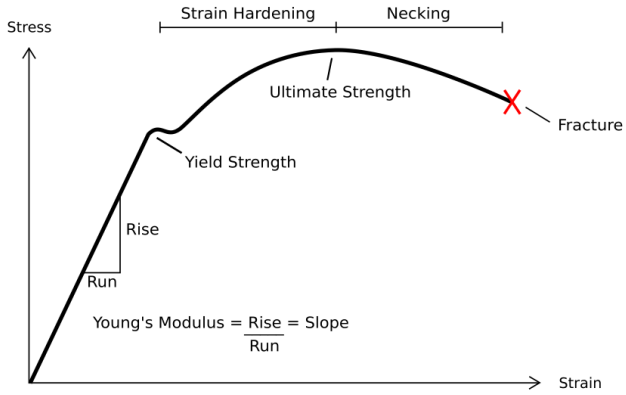

Figure 4.3: Relationship between stress and strain

The material will behave linearly in the first part. This means that the relationship between the strain and the stress is proportional and equal to a constant. This constant is the elasticity module (E), and as shown in the figure, is the slope. The material is linear until the stress reaches the yield stress, σ_y. If the strain is increasing further, the material will get a permanent and plastic deformation. When the strain decreases, the stress will follow a line parallel to the elastic curve back again.

Elastic-plastic material behaviour is often used in engineering to avoid the most complicated stress-strain relationship. After the stress reaches the yield strength, the material acts perfectly-plastic and the E-modulus will change, now being expressed as E_t. The relationship will still be linear after reaching the yield strength, but the slope has changed. Elastic-plastic material behaviour is often characterised by three rules, which sums up the above quite good:

1. The yield criterion: Linear behaviour until $|\sigma| = \sigma_y$, where non-reversible deformation occurs.

2. Hardening rule: Unloading after deformation follows the elastic E-modulus. Hardening can either be kinematic or isotropic.

3. Flow rule: Stress strain relationship after σ_y follows the plastic (tangential) E-modulus.

When unloading a material after yield, the hardening is said to be kinematic if unloading happens with a stress range being twice the yield stress, before it yields again. Isotropic hardening is defined as when the same stress range is defined as twice the current stress value when unloading happens.

4.6.2 Geometry

In linear geometrical behaviour, small displacements and rotations are being assumed. It then follows that the displacement is linearly dependent on the geometric stiffness. For cases where loads are creating large deformations, the change in geometrical stiffness has to be taken into account. To illustrated the point, two hinged truss-bars with a load R compressing both bars can be looked at. Truss bars cannot rotate, so bifurcation will not occur.

In Figure 4.4, the load R versus the displacement r is shown. As the force pushes down, it increases linearly in the beginning when the deflections are small. As the deflection becomes larger, the response becomes non-linear. It will not reach a limit point where the force will decrease. Flexible risers are normally not subject to large strains, as the bars are here, but this example shows a clear non-linear behaviour.

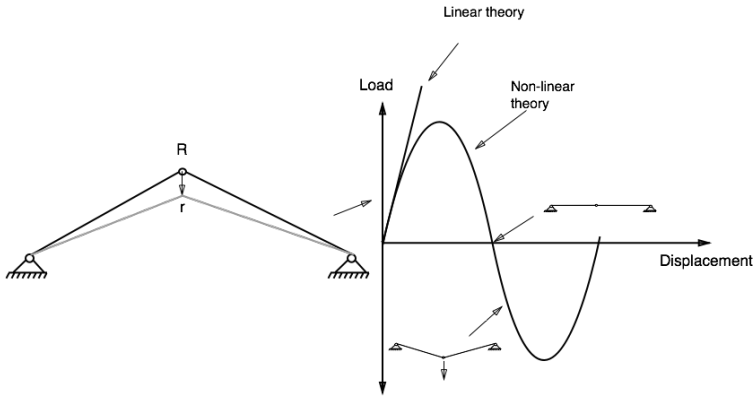

Figure 4.4: Simple two-bar truss example and the associated load-displacement relationship

4.6.3 Boundary

Non-linearity in boundary conditions is highly relevant for flexible risers. The critical point with regarding to high stress levels is typically at hang-off, where the riser is fixed. A bend stiffener or a bell mouth is therefore installed with the riser, in order to reduce the curvature. Both the bend stiffener and the bell mouth are examples that would lead to a non-linear boundary behaviour.

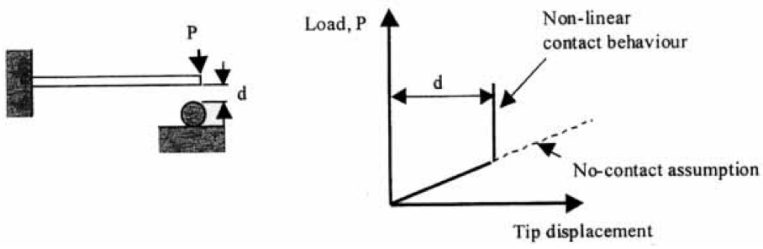

Figure 4.5: Example of non-linear boundary condition. Notice the sudden change in load-displacement relationship due to contact [Moan, 2003].

As can be seen in Figure 4.5, and analogously applied for a bell mouth, when the riser is bend it will at one point come in contact with the bell mouth, resulting in it being able to move further. The same applies for a bend stiffener, but in this case, the force will increase more gradually.

4.6.4 Hydrodynamic forces

Note that the drag term in Morsion's equation (Equation (4.1)), the last term in the equation, includes the response velocity of the cylinder. This is important to include for flexible pipes with a significant velocity, while not so important for stiff cylinders fixed to the seafloor. This can either be linearised using energy principles and solved analytically in the frequency domain, or solved numerically in the time domain.

4.6.5 Others

Interaction between the soil and pipeline can cause non-linear behaviour. For vertical motions, the seabed can behave elastically, while the friction factor can play a role if the movements are sideways. Either way can result in non-linear behaviour. In addition, the transported fluid can have high temperature, leading to non-linear phenomena like pipeline walking Sævik [2013].

4.7 Solution methods

The dynamic equilibrium equation can contain large matrices and non-linear relationships. Computational power is limited, so it is benefiting to solve these equation systems efficiently. Other important aspects of the chosen solution method are the stability and ability to provide an accurate answer.

4.7.1 Load incrementation methods

In structural engineering, load incrementation methods are most commonly used to determine the equilibrium position for a given load increment. Different methods are established, and among the most used methods in engineering is the Newton-Raphson and the Arc-length method.

The Newton-Raphson method is a less sophisticated method compared to the arc-length method, and can have problems solving some extreme non-linear problems. This is due to the stiffness matrix being singular where the first derivative is zero. The arc-length method avoids this, but will in return need more calculations to solve an equivalent problem. This method will not be further explained, as the focus is on solution methods applied by BFlex and SIMLA.

Newton-Raphson

This is an iterative method frequently used to solve non-linear problems in structural engineering. It is derived from simple geometrical considerations, and involves solving $f(x) = 0$. This can be expressed using the same response and load terminology as before and becomes Equation (4.4). The solution is also presented graphically in Figure 4.6.

$$\mathbf{r}_{n+1} = \mathbf{r}_n - \mathbf{K}^{-1}(\mathbf{r}_n)(\mathbf{R}_{int} - \mathbf{R}) \tag{4.4}$$

The advantage of this incrementation method is that the desired accuracy and hence the error can be made as small as necessary, since the equilibrium between the external and the internal forces are taken into account. However, this may take a significant amount of iterations, which increases the computational time. Computer programs normally have their own way of determining the desired accuracy, and in BFlex2010 and SIMLA, the user determines this.

As can be seen in the equation above, the stiffness matrix $\mathbf{K}(\mathbf{r}_n)$ is dependent on the response $\mathbf{r}_n$, and has to be calculated at every step. This process requires more computational time compared to computing the stiffness matrix less often. In Figure 4.7, two different methods of how to handle the stiffness matrix are compared. The first is the standard Newton-Raphson, where the stiffness matrix is updated after each iteration. If the stiffness matrix is large and complex, this

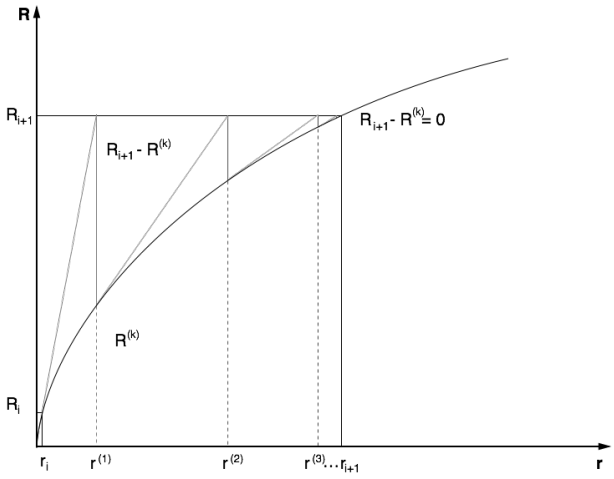

Figure 4.6: Iteration using the Newton-Raphson method

may be very time consuming. However, it requires less increments before the convergence criterion is met. The second method is a modified version of the Newton-Raphson method, where **K** is calculated only once. As can be seen, this method requires more increments. The method should hence be chosen based on the complexity of the stiffness matrix.

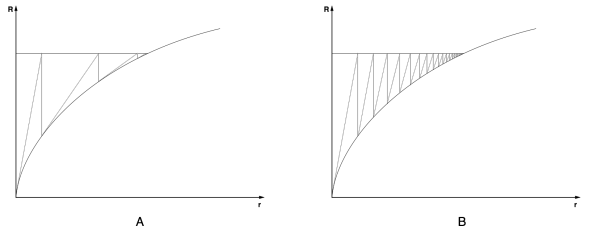

Figure 4.7: Comparison between no updating of **K** (B) and frequent updating (A)

4.7.2 Time integration methods

Time integration methods are divided into explicit and implicit time integration. Explicit integration expresses the displacement at the current time step as a function of the displacement, velocity and acceleration at the previous time step only. Implicit integration expresses the current displacement as a function containing known values at the previous time step in addition to unknown values at the current time step. This requires an equation system to be solved, and hence takes longer time to complete.

Some of the time integration methods are unconditionally stable. This means that the time step only affects the accuracy of the solution, and not the convergence. For methods that are not unconditionally stable, an important ratio as to if it converges is the h/T ratio, where h is the time increment and T is the eigenfrequency of the system. It should be controlled that this is sufficiently small.

The main time integration methods is the Newmark β-family, and the Hilbert, Hughes and Taylor (HHT-α) method. These will be further explained.

Newmark's β-family

Newmark's β-family can be derived by using a Taylor expansion, and leads to the two following two equations [Langen and Sigbjornsson, 1979]:

$$\dot{r}_{n+1} = \dot{r}_n + (1-\gamma)\, h\, \ddot{r}_n + \gamma\, h\, \ddot{r}_{n+1} \tag{4.5}$$

and

$$r_{n+1} = r_n + h\, \dot{r}_n + (\frac{1}{2} + \beta)\, h^2\, \ddot{r}_n + \beta\, h^2\, \ddot{r}_{n+1} \tag{4.6}$$

where h is the time step, r the displacement, $\dot{r}$ the velocity, $\ddot{r}$ the acceleration and n indicates time step number.

The two parameters γ and β can be defined by the user, according the desired stability and accuracy of the solution. According to Langen and Sigbjornsson [1979], by choosing $\gamma \geq \frac{1}{2}$ and $\beta \geq \frac{1}{4}(\gamma + \frac{1}{2})^2$ this method is unconditionally stable.

The γ-parameter expresses a mathematical damping of the system, and can be set according to the following guidelines. Note that in most situations, this value is set to one half:

$\gamma > \frac{1}{2}$ Gives a positive damping

$\gamma < \frac{1}{2}$ Gives a negative damping

$\gamma = \frac{1}{2}$ Gives no damping

As the name says, this method covers a family of different time integrations. Depending on what value is chosen for β, the method is identical to other known methods. Some of these includes the linear acceleration method ($\beta = \frac{1}{6}$) and the Euler-Gauss' constant average acceleration method ($\beta = \frac{1}{4}$).

A stability criterion, determining the lower limit as to whether the method is unconditionally stable, can according to Langen and Sigbjornsson [1979] be defined as

$$h_{cr} = \frac{T}{2\pi}(\frac{1}{4}(\gamma + \frac{1}{2})^2 - \beta)^{-\frac{1}{2}} \tag{4.7}$$

HHT-α method

Hilbert, Hughes and Taylor implemented numerical damping to control the solution in order to obtain an accurate solution. This is an implicit method, which is highly suitable for non-linear problems with poor convergence.

The HHT-α method are based on the same equation for displacement and velocity as the Newmark-method does, i.e. Equation (4.6) and (4.5). By introducing a third parameter α, the equilibrium is rewritten as [Sævik, 2010]:

$$\mathbf{M}\,\ddot{\mathbf{r}}_{n+1} + \mathbf{C}\,\dot{\mathbf{r}}_{n+1} + (1-\alpha)\,\mathbf{K}\,\mathbf{r}_{n+1} - \alpha\,\mathbf{K}\,\mathbf{r}_n = \mathbf{R}_{n+1} \tag{4.8}$$

This is the modified equation system that needs to be solved. The value of α is normally in the region between $0 > \alpha > -\frac{1}{3}$.

Chapter 5

Fatigue

5.1 General

Fatigue damage can be defined as cyclic loading leading to a degeneration of the material. This topic is important to consider in the design of flexible risers, as they are subject to a large number of cycles during their lifetime. These stress cycles are not critical as one, but added together the total damage can be a significant threat to the design life. There are different methods used to calculate the fatigue damage, but there is still an uncertainty that makes it hard to determine accurately how long the fatigue life will be. Fatigue is complicated process affected by many different factors, which means that today's calculation has to be on the conservative side.

Fatigue can normally be divided into two groups, based on the number of cycles before failure: Low-cycle and high-cycle fatigue. Low-cycle fatigue is mainly used when failure occur after approximately 10^4 cycles, and high-cycle when more than 10^5 cycles leads to failure. The stress range is normally in the elastic range for high-cycle fatigue, while it may exceed the yield stress in low-cycle fatigue.

5.2 Fracture mechanics

Fatigue damage and fracture mechanics are closely related. The tensile armours in the flexible riser are governed by fatigue of the material, but is affected by crack initiation and crack growth.

In a metal, some of the grains in the material will be aligned in the same microscopic plane as the maximum shear force. The material will hence be weaker in this plane. When this material is being subjected to variable loading, this plane will

slip, leading to what will develop to a microscopic crack. The crack growth rate can be described by using Paris Law [Almar-Næss and et al, 1985]:

$$\frac{da}{dN} = C(\Delta K)^m \tag{5.1}$$

where $\frac{da}{dN}$ is the crack growth rate, ΔK is the stress intensity range and C and m is material dependent parameters determined by experiments. It can be shown that this formula is equivalent to the SN-curve, which will be introduced in the following section. Fatigue and crack growth can both lead to failure as a result of cyclic loading, and is often co-existing.

5.3 SN-Curves

Most of the fatigue calculations are based on SN-curves. These curves have shown to give a decent approximation of the fatigue life. SN is an abbreviation for stress and cycles (N), respectively. SN-curves are generally most suited for high cycle fatigue, as the strain is kept well within the elastic range. Low-cycle fatigue tend to give stresses in the plastic range, and is better described by a strain based method [MSC Software, 2014].

Most of the SN curves are either linear or bi-linear when the axes are logarithmic. For fatigue calculations in air, the curve is typically bi-linear, with the second slope being low. This means that for small enough stress cycles, the number of cycles the material can endure is close to infinity. However, this is not the case when the material is being exposed to sea water. The slope of the SN curve is getting steeper, and it changes from bi-linear to linear, meaning that even smaller cycles will affect the fatigue life. This is illustrated in Figure 5.1.

This implies that when doing fatigue calculations on flexible risers, we can stick to a linear SN curve as long as the material under no circumstances are being exposed to sea water, or leakage from the transported fluid and through the thermoplastic layers into the tensile armour. What happens if the tensile armour get wets is that it triggers another failure mechanism, corrosion fatigue. This will be deeper explained in Section 5.8.

The relation between the stress range and the number of cycles can be expressed as

$$N_i = a(\Delta\sigma)^{-m} \tag{5.2}$$

where N_i is the number of cycles, $\Delta\sigma$ is the stress range and a and m are factors determined by experiments, and dependent on the material. For logarithmic axes, the slop of the diagram will be equal to $-1/m$.

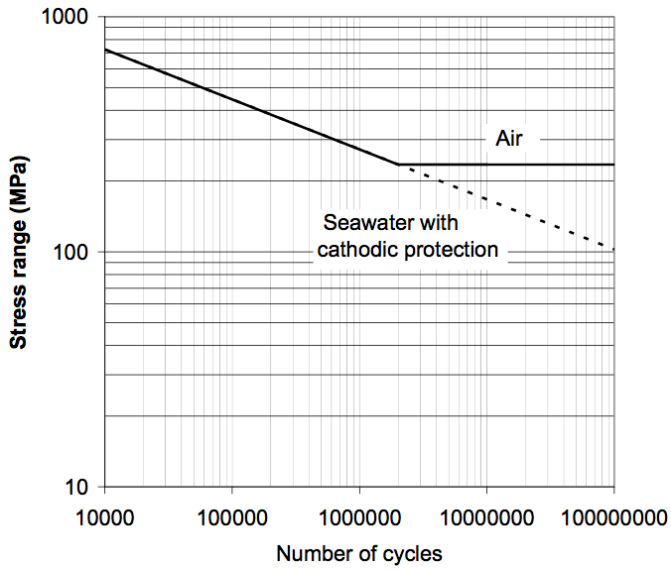

Figure 5.1: Example of how the SN-curve is different in air and seawater [DNV, 2012].

5.4 Miner's rule

There are many different proposals for how to calculate fatigue, but the most common is Miner's rule. This is being used due to its simplicity, and has proven to be no worse than other more sophisticated methods, due to the relatively large uncertainty coupled to fatigue.

This rule states that the damage per load cycle is equal to

$$D = \frac{1}{N} \tag{5.3}$$

where D is the damage and N is the total number of cycles the structure can handle at the given stress range. The total damage will then be the sum of all the cycles, given as

$$D_{tot} = \sum \frac{n_i}{N_i} \tag{5.4}$$

here, n_i is the number of cycles at the given stress range, and N_i is the number of cycles that would lead to failure.

The failure criterion when using Miner's Rule is that the total damage should be less than 1. In practice, this is typically set much lower to include a safety factor. Examples could be a total allowable damage of 0.2.

The advantage with this formula is it's simplicity and easy implementation into computer codes. The weakness is that it does not take the stress interaction into account, as cycles at a low stress range followed by cycles at a high stress range can give more damage than this rule predicts.

Once the damage is known, the expected fatigue life can be calculated. Since the damage over a given time is know, one can easily find the total fatigue life.

$$\text{Life} = \frac{T}{D} \tag{5.5}$$

Here, D is the damage associated with the time T, assuming that the time interval provides a damage estimate which is representative for the components life.

5.5 Mean stress correction

Stresses in structures exposed to wave loads will clearly be alternating, due to the waves harmonic behaviour. The tensile armour in flexible riser will most likely always experience a positive tension force. This implies that the stress level will be alternating about a mean value. This is illustrated in Figure 5.2. The SN-curve only applies for a given relationship between the minimum and maximum stress, often with values so that the mean stress is zero. Alternating between a mean value would give a larger damage compared to alternating between zero.

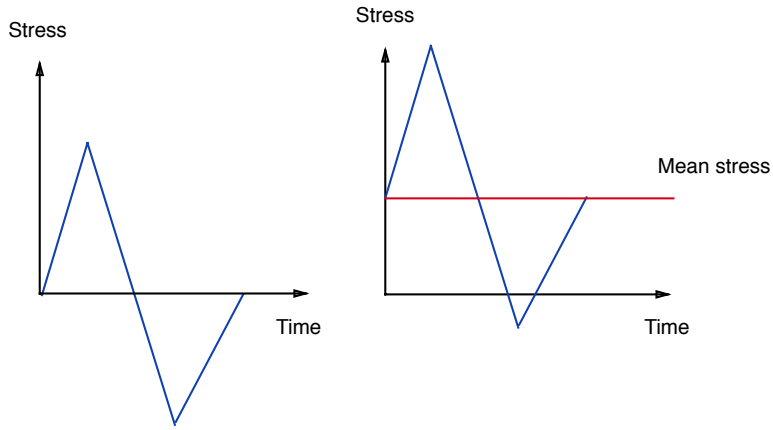

Figure 5.2: The two time series has the same amplitude, but different mean stress. This results in different damage.

A ratio R is often defined, which is defined as the relationship between the minimum stress (S_{min}) and the maximum stress (S_{max}):

$$R = \frac{S_{min}}{S_{max}} \tag{5.6}$$

This value will tell whether a mean stress correction is needed or not. If the R-ratio for the cycles is equal to the value the SN-curve applies to, no mean stress correction will have to be done. For different values, a mean stress correction should be done.

There are many different ways to do the mean stress correction. In fatigue calculations of flexible risers, the most common methods to account for this mean stress effect is to use either the Goodman relation or the Gerber relation. Figure 5.3 shows how these two methods differs. Basically, Goodman's mean stress correction assumes a linear relationship between the alternating stress and the corrected stress, while Gerber's correction assumes this to be a parabola.

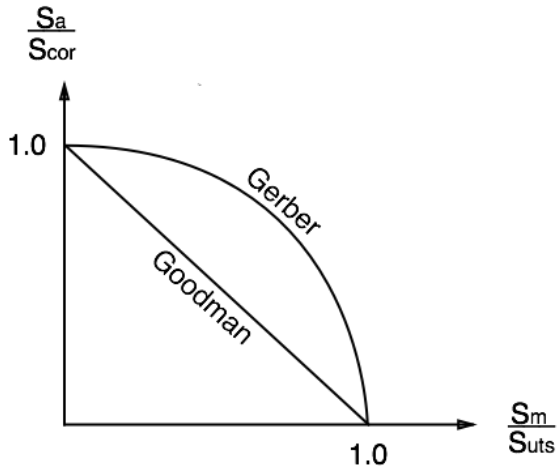

Figure 5.3: Comparison between Gerber's and Goodman's relation.

A general expression for the mean stress correction can be expressed as:

$$\frac{S_a}{S_c} + (\frac{S_m}{S_{uts}})^{fg} = 1 \tag{5.7}$$

where S_c is the corrected alternating stress, S_a is the alternating stress, S_m is the mean stress and S_{uts} is the ultimate strength. The factor fg is dependent on which method is used. If Goodman's correction is applied, the factor should be set to 1. If Gerber's relation is applied, the factor should be set to 2.

These methods are generally applied on different materials. The Gerber relation is the most suitable for ductile materials, while the Goodman relation is more suitable for brittle materials [Nieslony and Böhm, 2013]. The difference between Gerber's and Goodman's model is that in Gerber's model, it does not take into account if the material is being subjected to tension or compression. The Gerber relation has been used in the fatigue calculation in this thesis.

It is now possible to take the mean stress into account, and calculate how many cycles the material can sustain before failure:

$$N_c = N_i \cdot (\frac{S_c}{S_i})^m \tag{5.8}$$

where N_c is the number of cycles before failure with the mean stress taken into account, N_i is the original number of cycles before failure and S_i is the original stress amplitude where the mean stress has not been taken into account.

5.6 Rainflow counting

The forces acting on a pipe is stochastic of nature. This leads to the riser being subjected to varying stress cycles. As Miner's Rule only deals with a constant stress cycle, the stress history has to be divided into cycles with constant amplitude. Rainflow Counting (RFC) is a method for counting these different stress amplitudes.

The idea behind this method is: The stress history will be turned 90°, as illustrated in Figure 5.4. A rainflow is imagined being poured on the top, and based on the following rules, the total number of each corresponding group of mean stress and amplitude will be counted [Almar-Næss and et al, 1985]:

1. Rain is imagined flowing down the roof, initiating from the inside of each peak or valley. A peak is defined as where the first derivative changes sign from positive to negative, and a valley is defined as where the first derivative changes sign from negative to positive.

2. When the water reaches the edge, it will drip down. If it joins another flow, a cycle is completed.

3. If the flow comes opposite a higher peak than from which it started, it will stop, and a half cycle is completed. The same also applies if it comes opposite a lower peak than from which it started.

This can be implemented into an algorithm used to count all the cycles and half-cycles. The algorithm would need to at least return the mean value of the cycle, the range and whether it is a half cycle or full cycle.

The damage can be calculated by doing a mean stress correction and using the SN-curve.

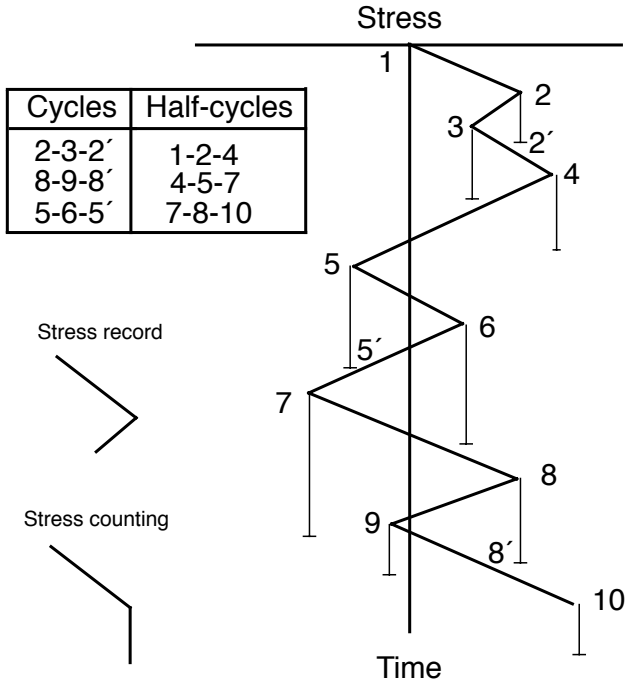

Figure 5.4: Rainflow counting of stress history.

5.7 Wave scatter diagram blocking

The wave scatter diagram can be used to perform fatigue analysis of a riser. This can be done if the wave height and period has been counted in a specific area. Once this is known, applying this sea state can give a quite good estimate of the real fatigue damage. However, these scatter diagrams consists of a large number of waves and corresponding periods, and it will take too long time to simulate every sea state. Use of wave scatter diagram is an useful way of determining the long term fatigue damage.

	Spectral Peak Period [s]																				
Hs	0-3	3-4	4-5	5-6	6-7	7-8	8-9	9-10	10-11	11-12	12-13	13-14	14-15	15-16	16-17	17-18	18-19	19-20	>20	SUM
0-1	55	426	1105	1561	1545	1228	649	536	319	182	101	55	30	16	9	5	3	1	2	8026
1-2	4	136	992	2957	5061	6057	5704	4553	3234	2113	1300	765	436	243	133	72	39	21	23	33843
2-3	0	5	104	678	2048	3703	4703	4670	3869	2606	1646	1127	650	359	192	100	51	26	26	26971
3-4	0	0	4	61	370	1108	2038	2639	2640	2178	1552	989	578	318	163	81	39	18	15	14788
4-5	0	0	0	3	37	208	613	1121	1438	1410	1125	765	459	249	125	59	26	11	8	7657
5-6	0	0	0	0	2	25	131	373	664	823	771	580	366	201	99	44	19	7	4	4109
6-7	0	0	0	0	0	1	17	83	225	380	444	387	267	153	75	32	13	5	2	2084
7-8	0	0	0	0	0	0	1	11	53	132	207	221	175	108	58	23	9	3	1	999
8-9	0	0	0	0	0	0	0	1	6	33	75	105	101	70	38	16	6	2	1	456
9-10	0	0	0	0	0	0	0	0	1	6	20	40	49	41	25	11	4	1	0	198
10-11	0	0	0	0	0	0	0	0	0	1	4	12	20	21	15	8	3	1	0	85
11-12	0	0	0	0	0	0	0	0	0	0	1	3	7	9	8	5	2	1	0	36
12-13	0	0	0	0	0	0	0	0	0	0	0	0	2	3	4	3	1	0	0	13
13-14	0	0	0	0	0	0	0	0	0	0	0	0	0	1	1	1	1	0	0	4
14-15	0	0	0	0	0	0	0	0	0	0	0	0	0	0	0	1	0	0	0	1
15-16	0	0	0	0	0	0	0	0	0	0	0	0	0	0	0	0	0	0	0	0
	59	567	2205	5260	9063	12330	14062	13987	12451	10066	7446	5049	3140	1789	942	461	216	97	82	99272

Figure 5.5: Example of wave scatter blocking [Sødal, 2009]

The idea behind the wave scatter diagram is to divide the sea state into a number of blocks, with a corresponding wave height and period. The total fatigue damage for each of the individual waves in one block should correspond to the total damage from applying the equivalent sea state a number of times. The damage from one block should not exceed 5-10% of the total damage [Sødal, 2009] . The advantage is that much shorter computational time is required to calculate the fatigue damage, and the result would still not be overly conservative. With today's computers consisting of many cores, the time used to simulate the corresponding load cases is acceptable.

5.8 Corrosion-influence on fatigue

Corrosion of the steel layers in a flexible riser is critical, as it can drastically reduce the fatigue life. The riser operates in an environment where many different corrosion mechanisms are present, so corrosion is not uncommon. The corrosive fluid can get in contact with the steel layers in different ways. If the external polymeric sheath gets damaged, seawater can seep into the tensile layers. The corrosive rate depends on a number of factors, such as the temperature and the oxygen level. Regular inspection of the riser is needed in order to make sure that the flexible riser's external sheath is intact.

Corrosion can also happen if gas from the internal fluid diffuses through the internal sheath. The two most common gases that leads to corrosion are either carbon dioxide or hydrogen sulphide [Smith et al., 2007c]. These two gases are present at either sweet or sour service, respectively. The corrosive rate is not high enough to cause failure by loss of steel. What happens is that these gases initiates micro cracks in the surface, which significantly accelerates the fatigue damage. Experiments done by Andersen [2002] have shown that the fatigue life can be reduced to between 2% - 10% of what it would be in air.

All risers have passive protection in the thermoplastic sheaths, and as long as

these stay intact and the annulus stays dry, corrosion should be under control. The annulus is most prone to come in contact with seawater during installation. Corrosion fatigue will have to be taken into account for cases where the annulus has or will become wet.

5.9 Fatigue analysis

Taking the bending hysteresis into account can be a computational demanding and time consuming task. In the past, fatigue analysis has been simplified by assuming a low, linear stiffness. Some have taken the structural damping into account by using either an equivalent viscous damping or Rayleigh damping, but in general the process has not been as transparent and equal as it should have been. Blocking of a wave scatter into regular waves along with Miner's rule to estimate the damage has lead to an overly conservative estimate of the fatigue life.

The progress of the computational power and available cores have increased significantly the last years, and this allows for more advanced calculations to take place. A recent Joint Industry Project (JIP) called Real Life has studied the different methods used for fatigue analysis, with the goal of establishing one unison standard. This new proposal has been submitted to API to be considered as an API standard. Smith et al. [2007a] have reviewed this work.

The reason for initiating this JIP is because of the lack of consistent methods used. There are several simplifications commonly made, which are directly influencing the fatigue life. Some of the most important are: Over-simplification of the global dynamic behaviour, neglecting wave directions, irregular waves and rainflow counting. Not taking the pipe damping, hysteresis effect or the non-linear moment curvature into consideration. Assuming the pipe annulus to stay dry and not taking into account the variation of stresses in the armour wires around the cross section.

The Real Life project recommends the fatigue analysis to be divided into the following six stages, as written in Smith et al. [2007a].

1. *Collate loading data*
2. *Define load case matrix*
3. *Riser structural design*
4. *Global analysis*
5. *Transposition from global to local*
6. *Local stress analysis*

This list is similar with the process of designing for extreme loads. The difference lays in that the transposition from global to local model should be carefully assessed, and the local model should be analysed with greater accuracy during a fatigue analysis.

Guidance and recommendation is given for each load step. Detailed information to identify the main factors is given, and provides a fundamental overview of how design for fatigue should be done. The final design is a result of an iteration process, and suggestion is given to improve the design if it proves to be unviable. For the complete list, see Smith et al. [2007a].

Chapter 6

Modelling and Analysis

This chapter defines the input used in the analyses, this includes the riser configuration, pipe cross-section properties, environment, hydrodynamic coefficients and vessel motion. The local model in BFlex and the global model in SIMLA is then presented. The analysis process used to obtain the fatigue data is found in Section 6.4.

6.1 Input

The main input data is provided by 4Subsea [2014], and where data are not complete, assumptions have been made.

6.1.1 Pipe data

The flexible riser studied contains polymer sheaths as well as pressure armour (zeta) and two tensile layers. The following layers and values are used in the BFlex analyses:

Layer	Thickness	E-modulus	Poisson ratio
Pressure liner	14 mm	300 MPa	0.4
Pressure armour	10 mm	210 GPa	0.3
Anti-wear tape	1 mm	300 MPa	0.4
Tensile layer 1	6 mm x 15 mm	210 GPa	0.3
Anti-wear tape	1 mm	300 MPa	0.4
Tensile layer 1	6 mm x 15 mm	210 GPa	0.3
External sheath	14 mm	300 MPa	0.4

Table 6.1: Pipe data

The inner diameter of the pipe is 270 mm. The internal pressure in the jumper is 200 bar. Tensile layer 1 contains 50 tendons and tensile layer 2 contains 52 tendons. The lay angle is 35 degrees, with opposite direction in each tensile layer.

In addition, the fatigue data of the steel used in the riser is:

Property	Value
m	4
log(a)	18
Ultimate tensile strength	1200 MPa

Table 6.2: Fatigue properties of steel in tensile layers

m and log(a) refers to the constants used in Equation (5.2).

6.1.2 Configuration

The configuration looked at in this thesis is a jumper connected from a fixed platform to a vessel. This can be seen in Figure 6.1

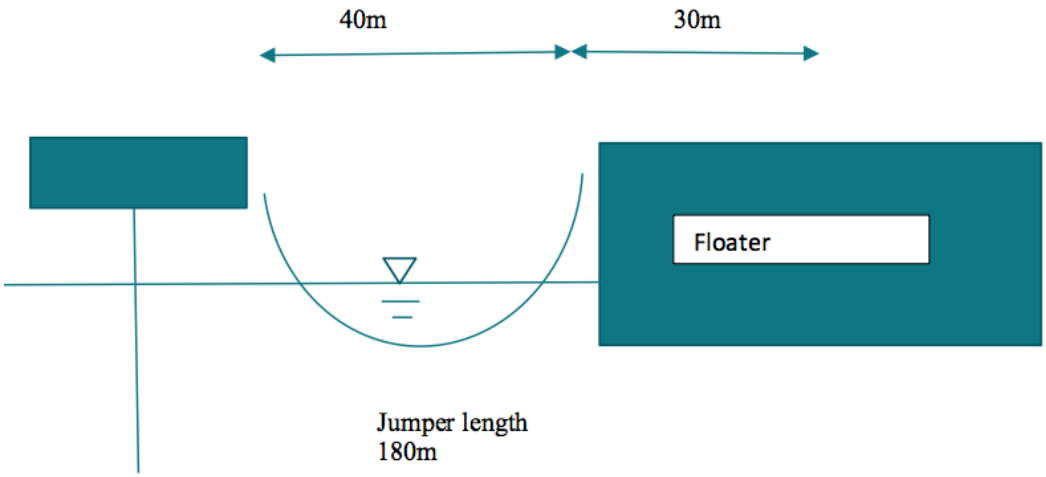

Figure 6.1: The configuration of the jumper

The jumper length is 180m, where one end is connected to the fixed platform 28 meters above sea level. The other end is connected to a floating vessel, 28 meters above sea level and centre of gravity of the vessel, with a distance of 30 meters horizontally. The distance between the two hang-offs is 40 meters.

6.1.3 Bend stiffener

Both ends are fixed with a bend stiffener, having the same geometry and elasticity. The bend stiffener is assumed to behave linearly. Figure 6.2 shows the bend stiffener, and bend stiffener data is given in Table 6.3.

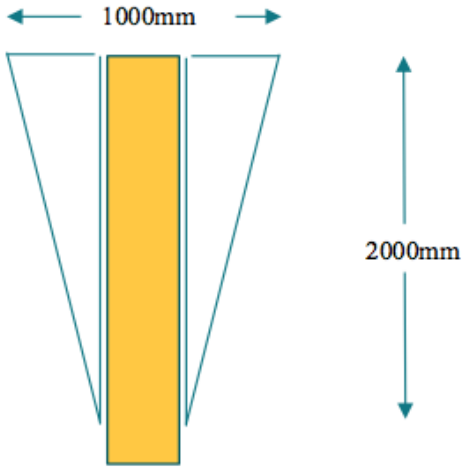

Figure 6.2: Bend stiffener geometry

Property	Value
Length	2000 mm
Outer diameter fixed end	1000 mm
Inner diameter fixed end	384 mm
E-modulus	154 MPa

Table 6.3: Properties of the bend stiffener

6.1.4 Environment

Both regular waves and irregular waves are being applied. For the regular case, Table 6.4 presents the wave heights, periods and number of waves that are being applied. The water depth for both cases is 150 meter.

Load case name	Wave height	Wave period	Number of waves	Wave direction
LC1	1.0 m	4.0 s	$3.4 \cdot 10^6$	0 deg
LC2	2.0 m	4.5 s	$2.2 \cdot 10^6$	0 deg
LC3	3.0 m	5.0 s	$1.0 \cdot 10^6$	0 deg
LC4	4.0 m	6.0 s	$4.0 \cdot 10^5$	0 deg
LC5	6.0 m	7.0 s	$8.0 \cdot 10^4$	0 deg
LC6	10.0 m	12.0 s	$1.0 \cdot 10^4$	0 deg
LC7	1.0 m	4.0 s	$3.4 \cdot 10^6$	45 deg
LC8	2.0 m	4.5 s	$2.2 \cdot 10^6$	45 deg
LC9	3.0 m	5.0 s	$1.0 \cdot 10^6$	45 deg
LC10	4.0 m	6.0 s	$4.0 \cdot 10^5$	45 deg
LC11	6.0 m	7.0 s	$8.0 \cdot 10^4$	45 deg
LC12	10.0 m	12.0 s	$1.0 \cdot 10^4$	45 deg

Table 6.4: Wave heights, periods, number of waves and corresponding load case number

For the irregular case, one sea state has been applied, using the JONSWAP-specter. Table 6.5 shows the sea state studied. Values are chosen based on an existing wave scatter diagram and to make sure that the hysteresis effect will be significant. The three parameters used in the JONSWAP-specter has been calculated based on the Equations given in the usermanual [Sævik et al., 2013b], which are functions of the given significant wave height and peak period.

Load case name	Significant wave height	Peak wave period	Wave direction	Duration
LC13	6.0 m	11.0 s	0 deg	500 s

Table 6.5: Significant wave height and peak wave period for irregular sea-state

Normally, a sea state lasting one hour would be necessarily to perform an adequate fatigue analysis [Sævik, 2014], but due to a computer problem, only 500 seconds have been simulated. This is done in agreement with the supervisor.

6.2 BFlex model

BFlex2010 is a finite element program suitable for detailed local stress and fatigue analysis of flexible pipes. It has a comprehensive element collection for multiple different analyses. The program is based on the work done by Sævik [1992], and a complete description of the program usage and theory can be found in Sævik et al. [2013a] and Sævik [2010].

The theory forming a basis for the understanding of BFlex can also be found in Chapter 3 and Chapter 4.

6.2.1 Stub-model

To perform a local analysis, a stub-model is created in BFlex2010 . This is a short model of the riser, consisting of very few elements. In this model, each layer and its interaction between the adjacent layers are being modelled much more detailed compared to the global model. The moment model is used, meaning that the tendons are modelled as a layer with a non-linear bending moment-curvature relationship, see Section 3.4.2.

The advantage of using a short model with few elements is of course the significantly reduced processing time. The disadvantage is that a global analysis has to be performed, in order to get information about the curvature, torsion and tension of the riser. It is necessary with a detailed model of the riser in order to get the correct stresses and a non-conservative estimate of the fatigue life.

6.2.2 Geometry and boundary conditions

Figure 6.3 shows the node and element definitions in the model. As can be seen in the figure, it consists of three nodes and two elements. The length of the stub model is 10 centimetres.

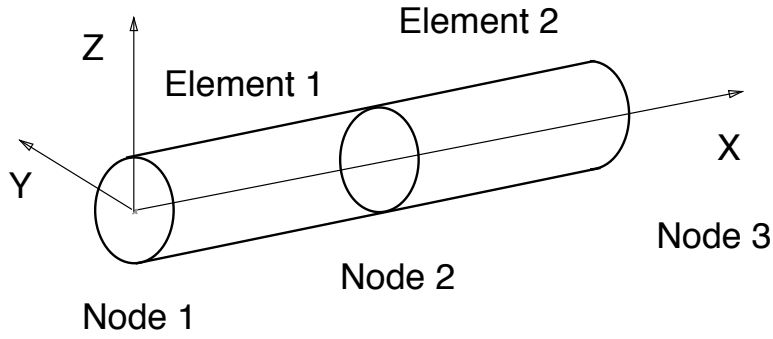

Figure 6.3: Shows the node and element numbering of the detailed local model, along with the coordinate system.

The boundary conditions are as following

- **Node 1** is fixed for translation in x-, y- and z-direction. It is free to rotate about the y- and z-axis, but fixed for rotation about the x-axis (to avoid singularity).

- **Node 3** is fixed for translation in y- and z-direction, while free to move in all other degrees of freedom.

A given rotation applied on both ends will result in a constant curvature over the cross section. Since the model is fixed for rotation at the first node, applying at rotation about the x-axis to the second node will result in a constant torsion over the length.

6.2.3 Elements and meshing

The BFlex2010 model is quite simple, only containing two elements. The element used is PIPE52, a three dimensional flexible pipe element with two nodes, and three integration sections along the element [Sævik et al., 2013a]. This element applies the moment model, and the bending moment versus curvature has been taking into account for both layers, i.e. ITCODE31 is used.

The element is divided into three integration sections, with a cross-section consisting of 16 integration points, as indicated in Figure 6.4a.

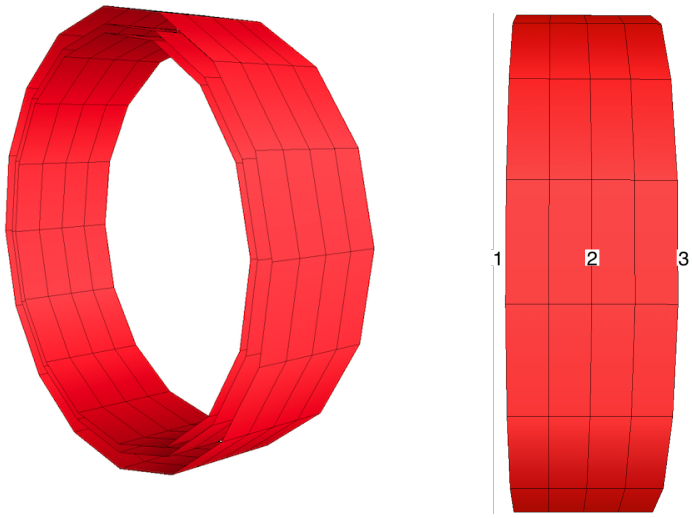

(a) Mesh of layers (b) Node numbers

Figure 6.4: BFlex2010 meshing and node orientations

6.2.4 Loads

BFlex2010 is used two times, for different purposes. The first time as a pre-analysis, only to calculate the pipe cross-section characteristics in terms of axial force versus

strain, torque versus torsion and bending moment versus curvature. The second time, output from SIMLA is used to calculate the stresses.

Pre-analysis

The axial force versus strain has been found be applying a given displacement to the stub-model, and printing out the corresponding axial force. The strain is then equal to the displacement divided by the length of the model (0.1m). Note that according to the Equation below, the slope of this graph will be the stiffness in axial direction

$$\sigma = E\,\varepsilon \implies \frac{F}{A} = E\,\varepsilon \implies F = EA\,\varepsilon \tag{6.1}$$

The relationship between the bending moment and curvature is defined in Equation (3.1). The relationship between the curvature and rotation can be seen in Equation (6.2), when a given rotation θ is applied with opposite signs to both ends. When the curvature and corresponding bending moment is known, the stiffness is easily found as the slope.

$$\kappa = \frac{2\theta}{L} \tag{6.2}$$

The same principles used to find the bending stiffness is analogously applied to find the torsional stiffness, by using the torque versus torsion relationship defined in the equation below:

$$M_T = GI_T \cdot \kappa = GI_T \cdot \frac{\theta}{L} \tag{6.3}$$

Main analysis

This analysis is carried out after each of the constitutive models has been used to analyse the global movements of the jumper. The curvature and tension history is now known for each element. These time series are now directly used as input to the local analysis. The tension and curvature values have been stored for each 0.1 second, and are given as input to BFlex2010 by using the THIST_F command. This will reproduce nearly the same movements in the local model, as the riser had during the global analyses.

6.3 SIMLA model

SIMLA is a finite element program that can be used to perform both non-linear static and dynamic analyses of pipes. In this thesis, SIMLA has been used to perform the global analysis of the jumper configuration. The primary output from this analysis has been the curvature and tension. A complete description of the program usage and theory can be found in Sævik et al. [2013b] and Sævik [2008].

6.3.1 Geometry and boundary conditions.

A static analysis is carried out to find the initial equilibrium position of the configuration. All the different constitutive models should have the same initial configuration, and this configuration is dependent on bending stiffness when the pipe is depressurised and no stick-slip effect is present. SIMLA uses Newton-Raphson iteration and the catenary equations to determine the initial position. The initial curvature of the non-linear model would have to be printed out, and using the INISTR command in SIMLA, the same curvature and hence initial configuration can be applied for both the non-linear and the linear models. The final static configuration can be seen in Figure 6.5.

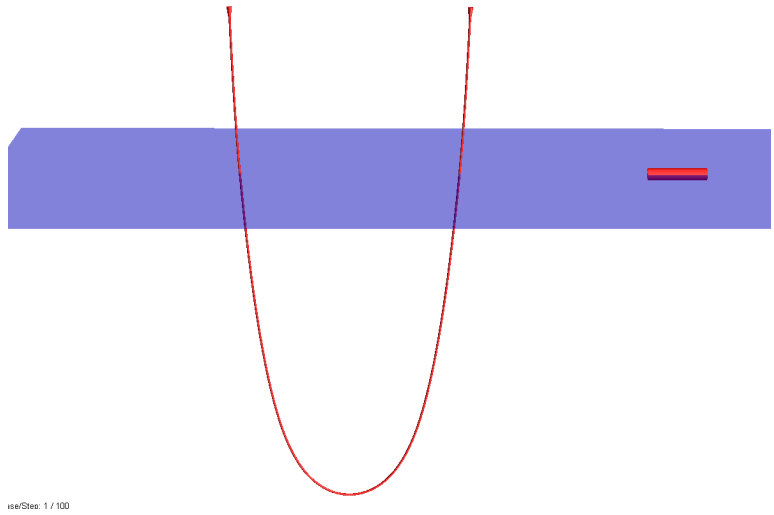

Figure 6.5: The static configuration of the jumper

Both ends of the riser are hinged during the static analysis. When the static equilibrium configuration is determined, a restart can be done to get the correct boundary conditions. The riser is fixed 30 meters above the sea level, 28 meter from the vessel.

6.3.2 Elements and meshing

Three different elements have been used to model the configuration. According to Sævik et al. [2013b], these elements have the following properties:

- PIPE31 is used in the linear model. This is a three-dimensional beam element with two nodes, where the axial and torsional strain is constant along the element.
- PIPE52 is used to model the bend stiffeners. This is a three-dimensional flexible pipe element with two nodes.
- COMPIPE42 is used in the non-linear model, and able the user to specify the axial, torsional and bending stiffness. This is also a three-dimensional beam element, with constant axial and torsional strain.

The main length of the element has been sat to 1 meter, except for critical areas where curvature and forces are expected to vary significant. The bend stiffeners have been identified as the most critical areas, where the number of elements is increased, and the element lengths decreased. Fine meshing here would lead to a more numerically stable model and more accurate results along the bend stiffener. The bend stiffener and meshing is shown in the Figure 6.6. Marked are elements that are further studied later.

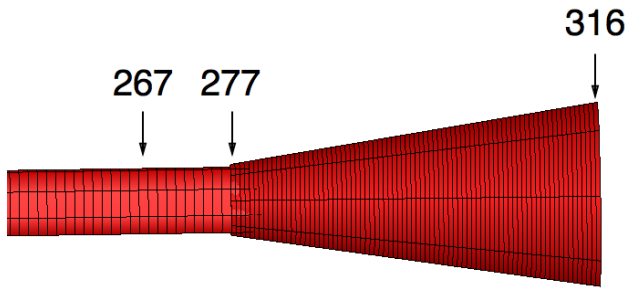

Figure 6.6: Meshing of bend stiffener, along with marking of important elements

The element length and number of elements at given positions are given below in Table 6.6. It should be noted that elements 277-316 are the bend stiffener connected to the vessel, as can be seen in Figure 6.6. These elements, in addition to ten more, are studied further in the fatigue analysis to capture the most critical fatigue point.

Element number	Element length [cm]	Number of elements	Position along riser
316 - 277	5	40	180-178m
276 - 257	10	20	178-176m
256 - 247	20	10	176-174m
246 - 242	40	5	174-172m
241 - 237	80	5	172-168m

Table 6.6: Element length and position, starting from the bend stiffener hang-off at vessel

6.3.3 Dynamic analysis

The dynamic analysis is done by restarting final configuration the jumper had when the static analysis is completed. Regular waves and irregular waves has been applied, according to the load cases defined in Section 6.1.4. In addition, the following list sums up the main aspects of the dynamic analysis.

- No current, marine growth or vessel offset has been applied.
- The hydrodynamic coefficients are given as 1.05 for drag and 0.6 for added mass.
- The wave loads have been applied over 40 seconds, this to avoid convergence problems if the wave load were too suddenly applied.
- The convergence ratio used is $1 \cdot 10^{-6}$
- The time steps used is 0.01 for the non-linear model and 0.1 for the linear model.
- The angle of the riser at hang-off is given the same angle as it got during the static analysis.

6.3.4 Vessel motions

The riser is connected to vessel, which movements are connected to the waves with an RAO (Response Amplitude Operator). The RAO says how much the vessel is moving for a given wave height, in a given degree of freedom. For waves in plane, the relevant degrees of freedom will be translation in x- and z-direction, along with rotation about the y-axis (surge, heave and pitch, respectively). For waves propagating in 45 degrees, it will in addition have translation in y-direction and rotation about the x- and z-axis (sway, roll and yaw). The movements of the riser will be coupled, since it is connected away from the centre of gravity of the vessel. The RAOs of the vessel can be found in Appendix B.

The advantage with regular waves, is that they can be described as a sinusoidal function. After a given time, the transients (time-dependent) factors will vanish, and the response will be regular as well. This means that a shorter time period needs to be simulated to calculate the forces. However, if the wave period is approximately the same as the eigenperiod of the vessel, resonance can occur. This leads to an amplification of the loads, meaning that smaller waves can give a higher damage than a large wave. In addition, there may be cancellation effects that affects the damage in the opposite way.

According to the RAOs, the vessel could be subject to resonance in heave for load case 5, although the response still will be mild. This seems to be the only resonance period that aligns with the wave periods.

6.4 Analysis method

This section is meant to describe the idea behind how the programs are being used to determine the fatigue damage. The main programs used are SIMLA, BFlex and MATLAB. The final solution is a result of a synergy between these programs. An illustration of this process can be seen in Figure 6.7.

The analysis method, described by words, is as following:

0. Establish a local stub-model of the riser using BFlex2010
A stub-model has been established in BFlex using the moment model. Here, the tendons in the tensile layers are modelled as individual layers, with the remaining layers have been modelled as a "core" layer. This core layers behave linearly, with a stiffness corresponding to the total stiffness of the polymeric and anti wear layers. The tensile layers have been given elastic material properties in BFlex, as it is assumed that the stress range is well within the elastic part of the material.

Correct pressure has been applied to the stub model, as well as a constant tension force. This tension force is equal to the average force the element is being subject to during a dynamic analysis. By applying a given displacement to the stub-model, the relationship between force and strain due to an axial load can be established. By applying a rotation, the same relationship for the torsional moment versus the rotation can be established. Finally, by applying a constant curvature, a bending moment-curvature diagram for the pipe cross-section can be established. These results can be used to establish the stiffness in the axial, torsional and bending degree of freedom, respectively.

Note that three different constitutive models have been studied, and the stiffness is dependent on these models.

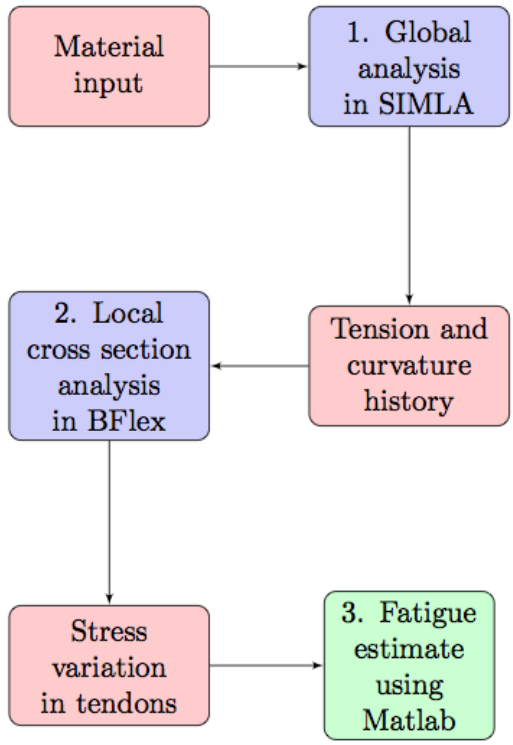

Figure 6.7: Flowchart showing the analysis process. Note that red color marks input/output, blue color is for steps involving computer analyses, and green marks the final result, the fatigue damage.

1. Global analysis using SIMLA
Once the material properties have been established, this can be taken as input by SIMLA. Depending on whether the non-linear or the linear constitutive models are being studied, different element types are being used (see Section 6.3.2). By using Cygwin, a total of 39 analyses will be run in SIMLA. The output from these analyses is the time variation of the tension and both the curvature about the y- and z-axis.

2. Local analysis using BFlex2010
Each element will now be analysed on a detailed level. A selection of 50 elements in the bend stiffener, and 22 elements along the sag bend will be studied, resulting in a total of 2742 cases to be run in BFlex2010 . The tension history and the curvature about both the y- and the z-axis can now be used as input to the local model. By post-processing the BFlex results file, the stress history can be found. Since the tendon has four corners, each of these corners have to be checked. In addition, the model has 16 integration points around the cross section where the stress has to be checked. By utilising symmetry, the number of integration points

can be reduced.

3. Fatigue analysis using MATLAB
The stress history can now be used to calculate the fatigue damage for each element, for all of the load cases. The stress series is corrected for with regard to the mean stress by using the Gerber relation, and then the specified SN-curve is applied to calculate the damage by using Miners rule. The damage per cycle is multiplied with the total number of cycles, leading to an estimate for the total damage.

For the irregular time series, rainflow counting is performed using the MATLAB toolbox provided by Nieslony [2009]. The damage for each different cycle is calculated, and the total damage for the sea state is found.

6.5 Assumptions

The following is a list containing the main assumptions made

- The length of the riser is relatively short, only 180 meters, and this means that the difference in external pressure along the length only is between 6-7 bars. The internal pressure is dominating with its 200 bars. The same moment-curvature relationship can therefore be applied for the whole riser length.
- The torsional moment and its effect on the stresses are neglected in the local model. This assumption can be justified when waves are in plane. The riser will probably experience small rotations about its longitudinal axis when the waves are approaching in 45 degrees, but the RAO for the vessel shows only small rotations in yaw.
- The moment model is used, meaning that the cross-wound armours are modelled as layers with a given moment curvature relationship. However, for fatigue calculations, it has proven to give a good fit with real test data [Sævik, 2011].
- When calculating the material properties in BFlex2010 , the tension force is assumed to be constant and equal to the average force the element experiences in a dynamic case. The varying force has been assumed to have little impact on the material curves.

Chapter 7

Results

7.1 General

This configuration has three critical areas on the riser where it is extra susceptible to high stress cycles, this being the two bend stiffeners and the sagging part at the middle of the riser. As reported by Smith et al. [2007c], the motion induced by heave, pitch and roll of the vessel is more significant than the direct action of waves on the riser. This, in addition to observing the stress during dynamic loading on the global model, lead to the elements at the bend stiffener attached to the vessel receiving the main focus with regard to the fatigue assessment. When referring to the bend stiffener later, the one connected to the vessel is being meant.

All the elements of the bend stiffener part of the riser is studied, as well as 10 elements further. This is 50 elements in total. The first element in the riser being covered by a bend stiffener is element number 277, and the riser element that is connected to the vessel is element number 316. (See Figure 6.6)

In the investigation of the tension and curvature behaviour, and when presenting the fatigue damage in tables, only a selected number of elements will be presented. This is due to the large amount of results stored for each element. These elements are:

- **Element 276**: This element is positioned 2.1 meter away from hang-off, and is chosen since it is the fatigue-critical element when the slip-stiffness is used.
- **Element 277**: Fatigue critical element when non-linear stiffness is used, and is the element which are positioned right inside the bend stiffener tip, 2.0 meters from hang-off.
- **Element 282**: This is the fatigue critical element when linear stick-stiffness is assumed, positioned 1.75 meter away from hang-off.

- **Element 315**: Second innermost element fixed to the vessel, 5 cm from hang-off.

The result from the fatigue analysis is presented as the total fatigue damage. One could easily find the fatigue life by taking the inverse of the damage multiplied by time, but this is not being presented.

7.2 Material curves

Below is the values used in the constitutive models. These are output from BFlex2010 , from applying a given displacement or rotation to the stub model. Hand calculations are also presented to verify the answers.

7.2.1 Axial and torsional stiffness

The following two graphs shows the constitutive relationship for axial and torsional loads, calculated by BFlex2010 . Notice that the slope is equal to the stiffness, when force versus strain and torsional moment versus rotation is on the y- and x-axis, respectively.

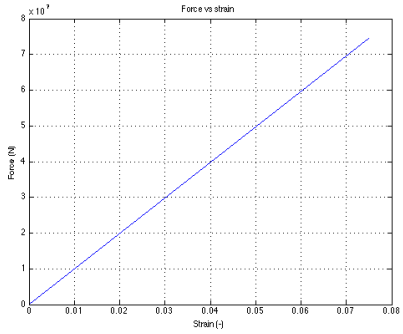

(a) Force vs strain

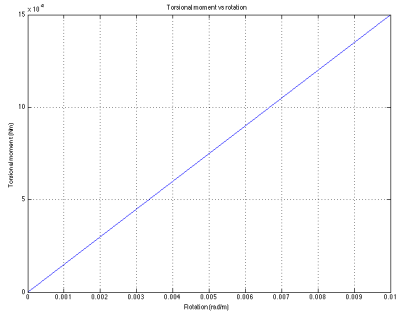

(b) Torsional moment vs rotation

Figure 7.1: Shows the material relationship for axial force and torsional moment

In the axial direction, the stiffness is 9.93 $\cdot 10^8$ N, and for torsion, the stiffness is 1.5 $\cdot 10^7$ N.

Hand calculations were performed to verify the answers, by using Equation (3.14) and (3.16). The results were a stiffness of 1.07 $\cdot 10^9$ in axial direction and 1.44 $\cdot 10^7$ N for torsion. The hand calculation seems to be in quite good agreement with the BFlex2010 results.

7.2.2 Bending stiffness

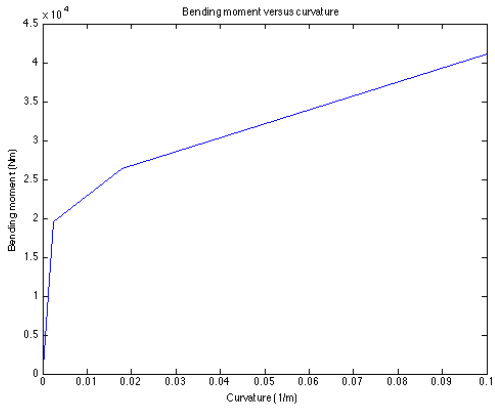

Figure 7.2: Non-linear relationship between bending moment and curvature

The slope before slip is $7.8 \cdot 10^6$ N and $1.786 \cdot 10^5$ N after full slip. The corresponding curvatures are 0.0025 m^{-1} and 0.01795 m^{-1}, respectively.

7.3 Regular waves in plane

The results in terms of dynamic response and fatigue damage for regular waves in plane are presented in this section. Where it is natural to present the difference for the three constitutive models for a given load case, load case number five will be presented. This corresponds to a wave height of six meter and a period of seven seconds.

7.3.1 Time consumption

All the analyses were timed, and the tables below show the time consumption for each step leading to the fatigue damage. This involves SIMLA calculations, BFlex calculations and post-processing of the stress history using a Matlab-script. It should be noted that the post-processing times below is valid for 50 elements processed. BFlex are doing calculations and post-processing of all the 50 elements, but only the last 20 seconds are stored to file. This time interval is large enough to at least catch the last stress cycle. This reduces the storage needed and also the computational time.

In addition, all the times should be looked at as guidelines and not absolute values. The processing time for the program was measured, and this should only give the

time the specified program uses. Running the same analysis two times could result in variation of the time, but it should nonetheless show the trend. The analysis is run on a laptop with an Intel Core i3 CPU, 2.4 GHz processor, 4MB RAM.

	Non-linear stiffness	**Linear stick stiffness**	**Linear slip stiffness**
Simulated time	**6x100s**	**6x100s**	**6x100s**
Calculations in SIMLA	513 min	39 min	51 min
Post-processing in SIMLA	5 min	4 min	4 min
Calculations in BFlex	150 min	150 min	150 min
Post-processing in BFlex	50 min	50 min	50 min
Calculations in Matlab	9 min	10 min	10 min
Total CPU time	727 min	253 min	264 min

Table 7.1: Time consumption for regular waves analyses, waves in plane.

The time difference in the BFlex2010 calculations and post-processing was negligible for the different models used. Due to a very similar time usage for each element, only a selected number of log files were checked and an average calculated. Based on this average, the total time was calculated. Since the stub-model consisted of very few elements, the speed was mainly dependent on how fast the hard disk was able to write, and not the calculations. Since the different models consisted of an equal number of tension and curvature values in the history file, the processing time was very similar. The same applies for Matlab, as the calculation time is independent on the different stress ranges.

7.3.2 Tension and curvature variation

Table 7.2 shows the curvature variation for the most fatigue critical elements, which is element number 276, 277 and 282, including the element at hang-off. The curvature range is being listed for the non-linear stiffness, and the two other models relative to the non-linear model. The average tension was very similar for each of the constitutive models, being about 92 kN. The curvature has been studied closer for this case, while the tension has been studied closer in the next section with waves in 45 degrees.

The difference in curvature for the three models in load case five can be seen in Table 7.2. The curvature of the linear models is given in per cent of the non-linear model, to indicate the differences more clearly.

Element	Non-linear stiffness	Linear stick stiffness	Linear slip stiffness
276	0.02713	29%	155%
277	0.02757	28%	150%
282	0.01779	42%	139%
315	0.00310	154%	98%

Table 7.2: Curvature variation for non-linear stiffness model, compared with the linear models. LC5. Unit: 1/m

The variation of history in time can be seen in Figure 7.3. Notice that while the linear models oscillates about a constant value corresponding to their initial curvature, the non-linear model have a clear shift in mean value.

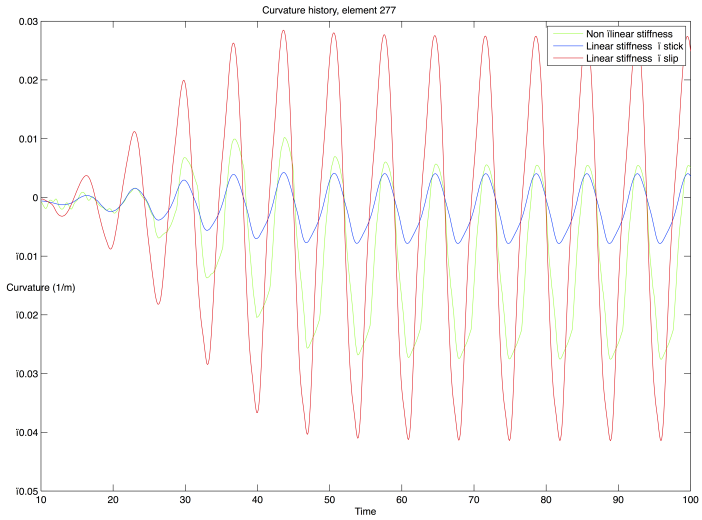

Figure 7.3: Curvature variation in time, for the different models.

7.3.3 Fatigue damage

The fatigue calculations have been performed by using the Gerber mean stress correction of the stress range, the SN-curve and finally Miner's rule to estimate the damage. The results from the fatigue calculations are presented here, for two locations. This is along the vessel bend stiffener area of the riser, and at the middle of the riser, called the sag bend. The fatigue fatigue data for all the load cases and models can be seen in Appendix A.

Fatigue was checked along the cross section integration points, in each corner of the tendons. For regular waves in plane, corner 1 and 3 had the same fatigue damage, and were the critical corners. For waves propagating in 45 degrees, corner 1 and 3 were still the most critical corners, but the fatigue damage in these corners were different dependent on the load case.

Bend stiffener at vessel

The results shows that the most critical position is at the bend stiffener tip. For the linear stick-stiffness model, the critical point has moved 25cm away from the tip, still in the bend stiffener. Figure 7.7 shows the fatigue damage of the riser along the bend stiffener for the non-linear model, while Figure 7.8 shows the same distribution, but for the linear slip-stiffness model.

These figures are shown as they are quite different, both regarding to how the damage is distributed and which load case gives most damage. The distribution for linear stick-stiffness can be found in Appendix A.1.

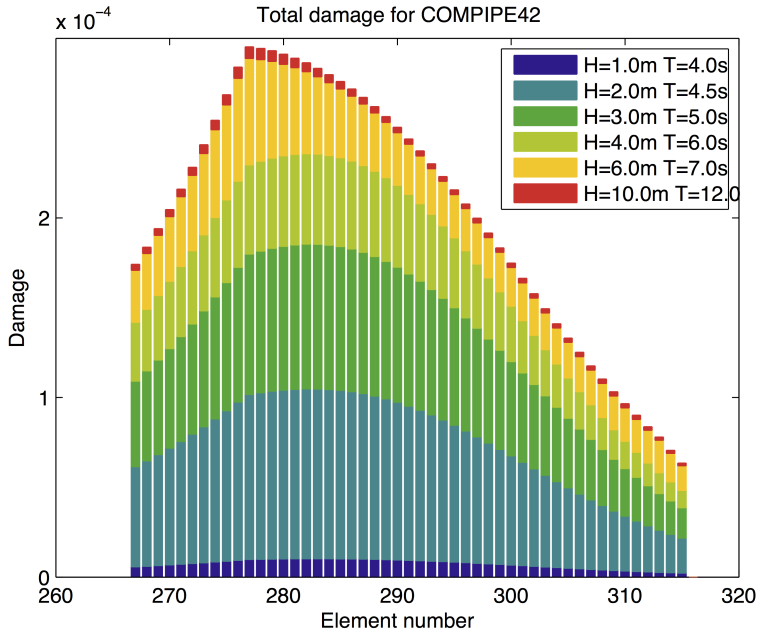

Figure 7.4: Damage distribution for non-linear stiffness, where element 277 is the riser at the bend stiffener tip and 316 is at the bend stiffener hang-off.

The damage is compared in Table 7.3, for each constitutive model.

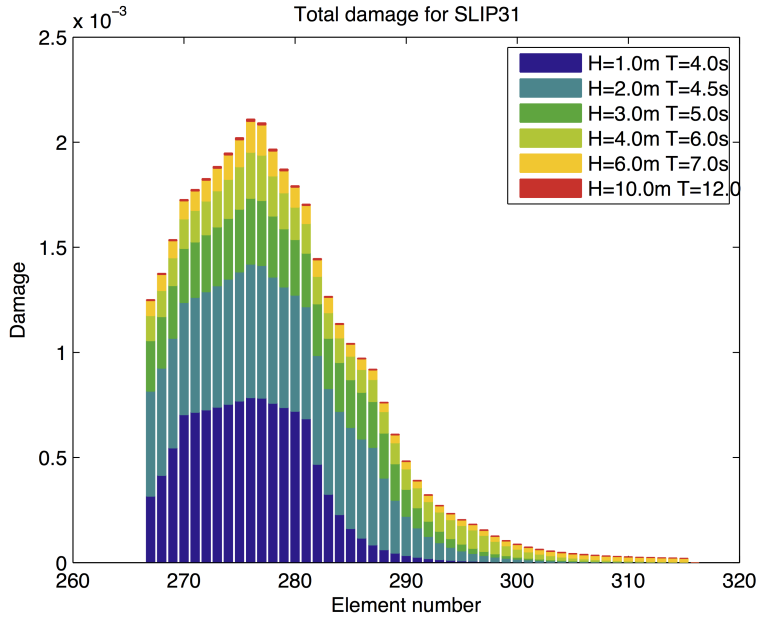

Figure 7.5: Damage distribution for linear slip-stiffness, where element 277 is the riser at the bend stiffener tip and 316 is at the bend stiffener hang-off.

Element	Non-linear stiffness	Linear stick stiffness	Linear slip stiffness
276	2.84e-4	82%	743%
277	2.95e-4	80%	709%
282	2.86e-4	85%	506%

Table 7.3: Fatigue damage for fatigue critical elements at bend stiffener, relative to non-linear stiffness.

In short, the non-linear stiffness gives a damage 24% higher than the stick-stiffness, and the linear slip-stiffness results in a damage 7 times greater. This value seems very high, but this is due to a large number of small waves not leading to hysteresis, and this is further discussed in Section 8.1.

The damage along the elements for each constitutive model is found in Appendix A.1

At sag bend

A total of 22 elements were studied at the sag bend. With an element length of one meter, this corresponds to 22 meters at the sag bend being checked. The fatigue critical spot along these elements was very dependent on the load case, and not as concentrated as in the bend stiffener. The element positioned 101 meter along the riser, starting at the platform hang-off was the most critical element of those studied. The damage here was about 8 % lower than in the bend stiffener.

Table 7.4 shows the damage at the middle of the riser, and 10 meter further, with linear damage relative to the non-linear damage

Element	Non-linear stiffness	Linear stick stiffness	Linear slip stiffness
158	9.0e-5	7.1e-5	1.65e-3
168	2.7e-4	2.53e-4	1.4e-3

Table 7.4: Fatigue damage for fatigue critical elements at the sag bend

The damage for the non-linear stiffness was 6.7% higher than the stick-stiffness, and the linear slip-stiffness was 6.1 times higher than the non-linear stiffness.

7.4 Regular waves heading in 45 degrees

The results in terms of dynamic response and fatigue damage for regular waves in plane are presented in this section. Where it is natural to present the difference for the three constitutive models for a given load case, load case number eleven will be presented, which corresponds to a wave height of six meter and a period of seven seconds. This is similar as load case five, but with a different direction (45 degrees). Keeping the wave height and period constant means that the results can be compared, to a certain degree, when the waves approach from a different direction.

7.4.1 Time consumption

Table 7.5 shows the time consumption for regular waves propagating in 45 degrees. The same general comments as for the time consumption for waves propagating in plane applies (Section 7.3.1).

	Non-linear stiffness	Linear stick stiffness	Linear slip stiffness
Simulated time	**6x100s**	**6x100s**	**6x100s**
Calculations in SIMLA	260 min	35 min	47 min
Post-processing in SIMLA	5 min	4 min	4 min
Calculations in BFlex	150 min	150 min	150 min
Post-processing in BFlex	50 min	50 min	50 min
Calculations in Matlab	8 min	8 min	8 min
Total CPU time	473 min	246 min	258 min

Table 7.5: Time consumption for regular waves analyses, waves 45 degrees

As can be seen, these analyses takes less time compared to when waves are propagating in plane.

7.4.2 Tension and curvature variation

The mean tension was very similar for the different constitutive models, being around 91kN. The linear stick-model had the lowest variation, the linear slip-model had the highest variation, and the hysteresis was placed in between these two models. It should be noted that the difference between these models was small. The tension is subject to further discussion in Section 8.3, due to small numerical problems.

Table 7.6 summarises the differences in curvature for the three constitutive models. The curvature range is presented, and as expected, quite different for each model.

Element	Non-linear stiffness	Linear stick stiffness	Linear slip stiffness
276	0.01836	31%	152%
277	0.01926	30%	143%
282	0.01496	39%	111%
315	0.00287	136%	75%

Table 7.6: Curvature variation for non-linear stiffness model, compared with linear models. Unit: 1/m

The maximum curvature variation for each model can be seen in Figure 7.6. Notice that slip is indicated when the non-linear model deviates from the stick-stiffness model. This happens from load case 3 when waves are propagating in 45 degrees.

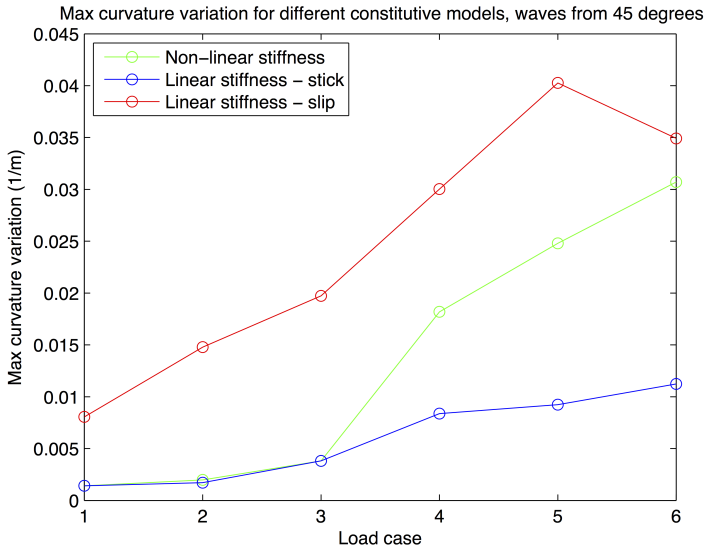

Figure 7.6: Curvature variation in element 277 for the three different models, for load case 7-12

The general trend in the curvature variation is quite similar to when waves were propagating in plane. The stick-stiffness model seems to be 30% of the non-linear model, and the slip-stiffness model is 1.5 times the non-linear model. This is valid for load case 5, but the values in per cent seems to be of about that order for all load cases where slip has happened.

7.4.3 Fatigue damage

The fatigue calculations have been performed by using the Gerber mean stress correction of the stress range, the SN-curve and finally Miner's rule to estimate the damage. The results from the two most critical locations along the riser are presented here: This is along the bend stiffener, and at the middle of the riser, the sag bend. The general trend is that the bend stiffener at the vessel is more critical than the sag bend.

Bend stiffener at vessel

The damage for the linear slip-stiffness model and the non-linear model is presented in Figure . These are the most interesting plots, as they compare current practice with the non-linear model. The damage distribution for the linear stick-stiffness can be found in Appendix A.2. The damage distribution and the critical spot can be seen in these figures, as well as the contribution from each load case.

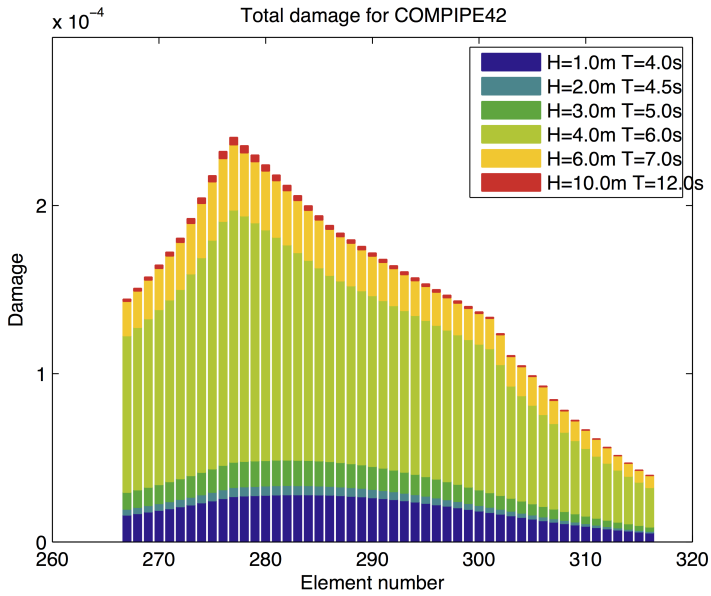

Figure 7.7: Damage distribution for non-linear stiffness, where element 277 is the riser at the bend stiffener tip and 316 is at the bend stiffener hang-off.

Numbers for critical elements are presented in Table 7.7. The damage is less than when waves were propagating in plane. The non-linear model gives 39% higher damage than for the stick-stiffness model. The linear slip-stiffness model gives a about 8 times greater damage.

Element	Non-linear stiffness	Linear stick stiffness	Linear slip stiffness
276	2.32e-4	73%	875%
277	2.41e-4	72%	826%
282	2.12e-4	82%	531%

Table 7.7: Fatigue damage for fatigue critical elements at bend stiffener, relative to non-linear stiffness

At sag bend

The fatigue critical location was not in the same position as for waves in plane. For the non-linear stiffness, and the linear stick-stiffness, the fatigue critical spot was much more defined as it was with linear slip-stiffness. Table 7.8 compares the damage in the two most critical elements

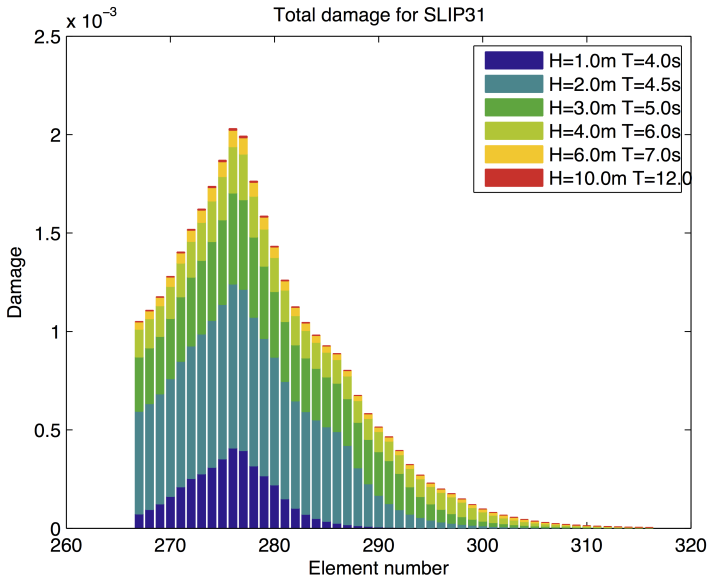

Figure 7.8: Damage distribution for linear slip-stiffness, where element 277 is the riser at the bend stiffener tip and 316 is at the bend stiffener hang-off.

Element	Non-linear stiffness	Linear stick stiffness	Linear slip stiffness
155	7.2e-5	4.4e-5	2.1e-3
156	5.6e-5	3.3e-5	2.1e-3

Table 7.8: Fatigue damage for fatigue critical elements at the sag bend

Non-linear stiffness gave a damage that is 63% higher than with the linear stick-stiffness.

7.5 Irregular waves in plane

Below are the results from the irregular analysis. The sea state was applied using a JONSWAP specter with a significant wave height of 6 meters, and a peak wave period equal to 11 seconds. The total simulation time of the sea state was 500 seconds. Finding the static equilibrium position and applying the waves smoothly was included in these seconds. Normally, it would be required to simulate an hour, but due to a computer problem, this could not be done. The damage is scaled to be equivalent to a one hour long sea state.

7.5.1 Time consumption

Below is the time used for calculations and post-processing for each program. It should be noted that the non-linear stiffness needed 0.01 second time steps to avoid numerical problems, while for the linear stiffness, 0.1 seconds seemed to be adequate. This resulted in that a complete non-linear analysis taking about 2.5 times longer to complete. The main difference lies in the time used by SIMLA, which is about 6 times longer for the non-linear analysis, as the time differences in BFlex2010 and Matlab for each constitutive model were negligible. Note that 50 elements (runs) are done in Bflex.

	Non-linear stiffness	**Linear stick stiffness**	**Linear slip stiffness**
Simulated time	**500s**	**500s**	**500s**
Calculations in SIMLA	637 min	99 min	121 min
Post-processing in SIMLA	10 min	7 min	7 min
Calculations in BFlex	192 min	192 min	192 min
Post-processing in BFlex	21 min	21 min	21 min
Calculations in Matlab	6 min	6 min	6 min
Total CPU time	14,4 hours	5,4 hours	5,8 hours

Table 7.9: Time consumption for irregular waves in plane.

7.5.2 Tension and curvature variation

The general trend for this sea-state seems to be that the non-linear model experiences about 15% more variation in tension than the stick-stiffness model. Compared to the linear slip-model, the tension variation is about 10% lower in the non-linear model. This is only valid for this specific load case. The mean value is of the same order for all the different models.

Element	**Non-linear stiffness**	**Linear stick stiffness**	**Linear slip stiffness**
276	0.047322	0.011060	0.059073
277	0.047830	0.011227	0.058449
282	0.029914	0.011637	0.035453
315	0.004593	0.007890	0.004582

Table 7.10: Curvature variation about the y-axis for the three constitutive models Unit: 1/m.

The curvature variation for each of the constitutive models can be seen in Table 7.10. The non-linear model experiences a curvature variation, in the fatigue critical

elements, of 3.3 times the variation in the linear stick-model. Compared to the linear slip-model, the max curvature variation is about 80% in the non-linear model.

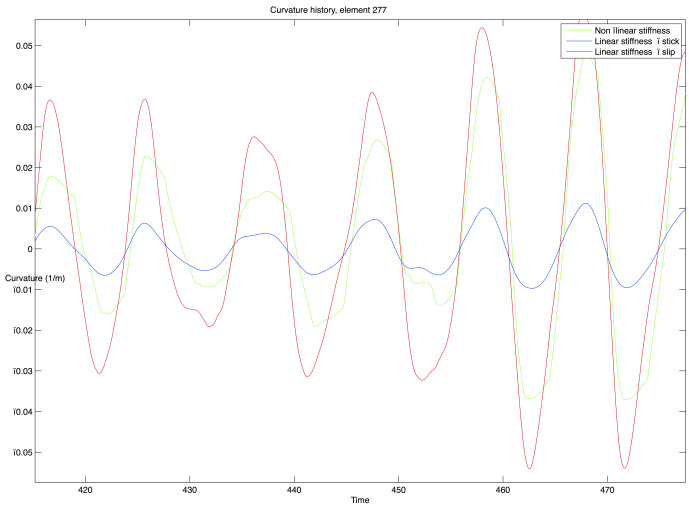

Figure 7.9: Shows the curvature variation for each constitutive model in element 277, for a selected time period.

7.5.3 Fatigue damage

The estimate for the fatigue damage should be a result of blocking the whole wave scatter diagram. In this case, only one sea state is studied, which seems to give an unrealistic result. The maximum damage occurring along the riser is given in Table 7.11. Since the damage proved to be higher in the bend stiffener than at the sag bend for the regular waves, this was the area being studied during the irregular wave analysis. All corners along with the most important integration points along the cross-section were checked.

	Non-linear stiffness	**Linear stick stiffness**	**Linear slip stiffness**
Max damage	5.8e-10	1.8e-12	1.3e-8

Table 7.11: Fatigue damage for irregular sea state

The linear slip-stiffness model gave a much higher damage than the other two models. The non-linear model gave a damage that was much closer to the linear-slip model than the linear stick-model. This indicates that the layers along the bend

stiffener tip slip most of the time. It should be noted that this is a sea-state that would occur more seldom. The results are subject to further discussion in Chapter 8.2.

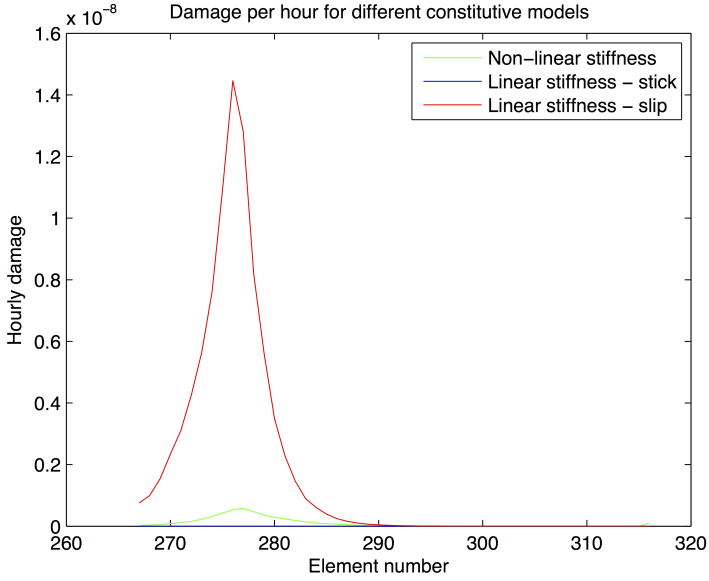

Figure 7.10: Comparison of damage distribution in the different constitutive models

Chapter 8

Discussion

This chapter will be split into three different sections. The first chapter will contain discussion about the observations done during the regular wave analysis. The second one will discuss the results obtained from the irregular wave analysis, and the third will discuss numerical problems and their influence on the results.

8.1 On regular waves

Time consumption

Three different programs have been used, and the time used by each program was stored. The results showed that the main difference in time consumption between the three models occurred in the global analysis. The non-linear model took up to ten times longer time in SIMLA, when regular waves were used. Non-linear analyses require more iteration, and often more advanced solution techniques as well. The linear analysis could be run with a time step of 0.1 seconds without problems, while several time test runs determined that 0.01 seconds resulted in the shortest CPU time for the non-linear model. The time used by BFlex was mostly limited by the time it takes to write the results to file, and is thus more dependent on the hard disk performance, and not which model were used. The total time needed to calculate the fatigue damage using each of the constitutive models showed that a non-linear analysis took approximately three times longer.

General on curvature

The curvature was equal for the non-linear and linear stick-stiffness model when the wave height was sufficiently small. Six different regular waves were studied, with two different wave headings. The results showed that for waves propagating

in plane, the non-linear model remains in the stick regime until the wave height exceeds four meters. Due to more motion at the hang-off when waves are propagating in 45 degrees, the hysteresis was present when the wave height exceeded three meters in this direction. The general trend in curvature variation showed that the linear stick-stiffness model had the lowest value, being about 30% of the variation in the non-linear model when waves were six meter high and had a period of seven seconds. For the same load case, the linear slip-model had a curvature variation that was 50% larger than the non-linear model. These ratios depend on how large the wave height is, and for an increasing wave height, the non-linear model will have a curvature variation that will converge against the linear slip-stiffness model.

When hysteresis is present, the curvature experienced a shift in the mean value to a non-zero value. This can be explained by the nature of an hysteresis loop. When the external loads are large enough to exceed the slip bending moment, the layers will slip. Since slip leads to a much lower stiffness, it will experience a rapid change in curvature. When the external forces decreases again, the equilibrium position for the bending moment can now be found at a non-zero curvature value. This means that hysteresis can be identified by looking at the curvature history. The degree of hysteresis can be determined by how large the shift in mean curvature is.

General on tension

The mean tension showed only small variations for each model, so this seemed to be unaffected by the different models used. The forces are subject to further discussion in the Section 8.3, as they had occasional peaks indicating a numerical problem. This had impact on the tension variation numbers, as the maximum tension was (incorrectly) taken at these peaks. The tension history was manually examined, and by neglecting these peaks, the behaviour followed the same general trend as for the curvature. Smaller stiffness will naturally lead to larger movements, and larger forces in the elements.

Both the results of the curvature and tension is as expected, as the stiffness has an direct impact on the movements of the riser when it is being subjected to wave loads and vessel motions. The linear stick-model experienced smallest variation and the slip-stiffness model experienced the highest variation in both tension and curvature. The non-linear model was placed in between the response of these two linear models, for most of the load cases closer to the stick-stiffness model.

General on fatigue

Regular waves in plane resulted in the highest fatigue damage. The total yearly damage was 24% higher for the non-linear stiffness model, compared to the stick-stiffness model. This difference in fatigue damage is a result of the hysteresis effect occurring in the non-linear model, as no hysteresis would result in an identical

response. The hysteresis has significant influence on the damage. The linear slip-stiffness model gave a damage 7 times greater than the non-linear model. This difference can indicate two things: Either, not much hysteresis is present, or there are a few number of waves leading to hysteresis.

By taking a look in which load cases contributes to the damage (see Section 7.3.3), it can clearly be seen that the main contribution to the fatigue damage in the linear slip-stiffness model comes from the first two load cases. In the non-linear model, the first load case barely contributes to the damage at all, resulting in very different results. This can be further verified by comparing the total yearly damage with the damage resulting from one wave, see Figure 8.1.

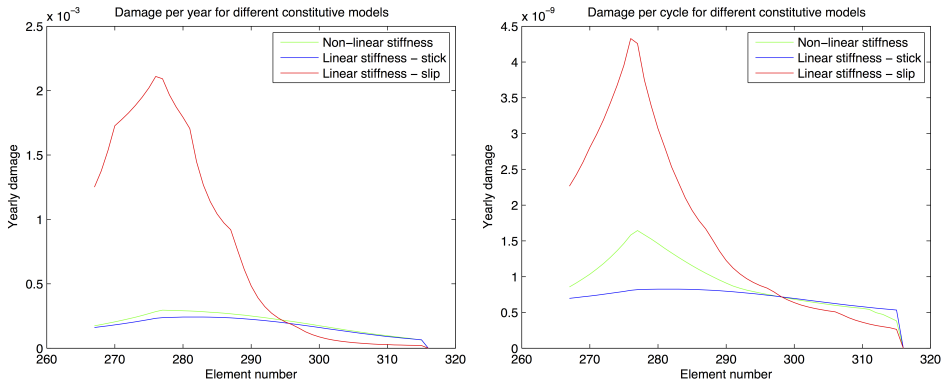

(a) Scaled with number of waves for each load case

(b) Scaled with one wave from each load case

Figure 8.1: Shows how the number of waves in each load case affects the total damage

The numbers of small waves not leading to hysteresis are in a clear majority, and this is where the non-linear model behaves equal to the linear stick-stiffness model. In addition, due to the low stiffness in the linear slip-model, the number of waves will lead to an significantly amount of damage being generated in this model.

It can be observed that if the load cases had consisted of an equal number of waves, the non-linear model would predict a damage twice the predicted value when using linear stick-stiffness. The linear model would only predict three times the damage as the non-linear model. This is however not so realistic, but gives a perspective on the minimum difference between the non-linear model and the linear slip-model.

Damage distribution and critical spots

The fatigue critical area for both wave directions was the bend stiffener. For regular waves in plane, the damage was at minimum 8% lower in the sag bend, and

significantly lower when waves approached in 45 degrees. The corners that were most fatigue critical were corner 1 and 3, dependent on the load case. While the maximum damage in the bend stiffener was clearly defined, the maximum damage along the sag bend were unevenly spread out with no clear fatigue hotspot. The element size in this area was one meter, and it could be an idea to decrease this length along the sag bend, to see if this has a positive effect on deciding the fatigue critical location. If the fatigue damage along the sag bend was more concentrated to one location, and not dependent on the load case, this could fast become the most fatigue critical area for this wave direction. Further studies should not underrate a more thorough check of the sag bend.

The three different constitutive models gave a different damage distribution along the bend stiffener. Both the non-linear and the slip-stiffness model predicted the fatigue critical spot to be close (or in the adjacent element) to the bend stiffener tip. This is what should be expected. The stick-stiffness model predicted the critical spot to lay 25 centimetres from the bend stiffener tip, inside the bend stiffener, and was also the model where the fatigue damage was most evenly spread out. The linear slip-model showed a drastic concentration of damage in elements near the bend stiffener tip (see Appendix A), while the non-linear model had the most intuitive distribution of damage.

Note that for the stick-stiffness model, the fatigue damage in the connection to the vessel was higher compared to the two other models. This is also as expected, as the stiff riser will have a more constant curvature along the length. The bend stiffener will then take less of the bending moment since the movements are smaller. When the riser using the linear slip-stiffness model is interacting with the bend stiffener, the bending moment will have to be balanced by a smaller moment at hang-off, leading to a smaller curvature and less damage.

Effect of wave direction on curvature and damage

The six different wave heights and periods were applied from two different directions, propagating in plane and in 45 degrees. As introducing waves in 45 degrees leads to translation in and rotation about all axes, this was expected to lead to a larger curvature variation, and hence an increased damage. The results showed that the layers slipped when the wave height exceeded 3 meters, while for waves in plane the layers slipped when the wave height exceeded 4 meters. This is most likely due to the vessel-induced motions at hang-off being larger when waves are propagating in 45 degrees.

The increased motion when waves propagated in 45 degrees resulted in an earlier slip between the layers. However, the damage was 13% lower than when waves propagated in plane. These numbers are contradictory, as an earlier slip would lead to the hysteresis effect to be more prominent, and hence have a larger damage. By studying the curvature variation for load case five and eleven (same wave height and period, but different heading), it can be seen that the curvature variation is

much greater for waves in plane. This can be seen in Table 7.2 and Table 7.6. This can be explained by looking at the RAOs in Appendix B, which indicates that the vessel is subject to larger heave movements for waves in plane, most likely due to a resonance effect. In addition, if the wave loads are more in phase with the vessel-induced motions at the bend stiffener when waves propagates in 45 degrees, this could lead to a smaller curvature variation.

These results display one problem about using regular waves, and this is the occurrence of resonance. For an irregular sea-state, resonance would be much less present due to constantly different waves. This means that if irregular waves were applied, the fatigue damage would most likely be more critical when was propagating in 45 degrees, due to the increased movements at hang-off.

Waves propagating in 45 degrees leads to an increased difference in damage between the bend stiffener and the sag bend, compared to when waves propagated in plane. This is because the increased vessel-induced motion mostly affects the curvature at hang-off, and not at the sag bend.

Contribution to total damage from each load case

The contribution from each load case when waves were propagating in plane seemed reasonable, taking into account the different numbers of waves and how the wave height was affecting the stresses. When waves were propagating in 45 degrees, the damage contribution from each load case was harder to predict, and is hence devoted a paragraph. Load case ten (wave height of four meter and period of six seconds) has the largest contribution to the total damage, when waves propagate in 45 degrees. This is a combination of several factors: This is the first load case where hysteresis is present, and there are still a significant number of waves to make sure that it is weighted enough to contribute significantly to the total damage. The load cases with lower wave height have much smaller stress variation due to no hysteresis. Load case one has a quite large contribution to damage compared to load case two and three. Since hysteresis is not present in any of these, all will be in the stick regime. The vessel motion is quite small for all of these wave heights, and since the first load case has the most waves, it is weighted more.

8.2 Irregular waves

Time consumption

Taking the non-linear behaviour into account when performing an irregular analysis in SIMLA took almost three times as longer than the linear models. If one hour is to be simulated, the total time for this riser system, including calculations in BFlex2010 and post-processing, will be around four days for one sea-state. A dedicated analysis computer can run all of the required sea-states on multiple cores,

meaning that a blocking of a full wave scatter diagram can be run in four days. In addition, an analysis computer will most likely be faster than the computer used to obtain the results in this thesis. Taking the non-linear behaviour into account should therefore be a realistic option with regard to time consumption.

General on curvature and tension

The max curvature range, using the non-linear model, was about 80% of the linear slip-stiffness model. This indicates that bending hysteresis must be present, due to its similarity with the slip-stiffness model. In addition, the non-linear model had a maximum curvature which was about 3.3 times higher than the linear stick-stiffness model. Because of this, one would expect that the fatigue damage using this irregular sea state would result in the fatigue damage being of the same order for the non-linear and linear slip-stiffness model. However, this is only the maximum recorded curvature range during 500 seconds, and does not say anything about how frequent this range occurs. The mean tension had only small differences between the models, but is subject to further discussion in Section 8.3.

During the last 40 seconds of the time series, the curvature is higher, and hysteresis is clearly present. This is where the maximum curvature occurs, and explains why the maximum curvature range is similar for the non-linear and the linear slip-stiffness model.

Fatigue damage

Figure 7.10 shows the damage for the three models. Even thought the maximum curvature range of the non-linear model only is 20% less than the linear slip-stiffness model, the damage is not similar. The linear slip-model predicts a damage over 20 times higher than using the non-linear model. This is due to several reasons. Hysteresis is present in most of the waves, but even though it is present, it is not experiencing the same curvature. For the highest wave, the curvature experienced by the non-linear model was 80% of the linear model. This follows that the stress in the linear-slip model always will be significantly higher.

In addition, it is worth noting that the non-linear model gives a much higher predicted damage than the linear stick-model. The damage is $5.8 \cdot 10^{-10}$ in the non-linear model and $1.8 \cdot 10^{-12}$ in the linear stick-stiffness model. These numbers are quite different, but they show that the majority of waves leads to hysteresis, as the non-linear stiffness predicts a damage closer to the linear slip-stiffness model.

From these results, although using the non-linear model gives much larger damage than the stick-slip model, it will still be a significant reduction in damage compared to the linear slip-stiffness model. In this case, one irregular sea state does not seem to give a realistic impression of the fatigue damage. Processing only 500 seconds of irregular waves did not seem to be enough. A full blocking of the wave scatter diagram would lead to a more proper weighting of this damage, as this is one of

the sea states that would most likely occur less. Further research has to be done on including the hysteresis effect in irregular sea-states.

As the results showed in the regular case, waves propagating in 45 degrees will lead to larger motions at the bend stiffener. The irregular analysis should therefore be considered to be run with waves propagating in this direction. The irregular waves would avoid amplification of the loads due to resonance.

Damage distribution and critical spot

The damage distribution showed the same general trend as for the regular waves. Both the non-linear and the stick-stiffness model tends to predict the damage to be more evenly spread over the bend stiffener, while the linear slip-stiffness model predicts a large concentrated damage around the bend stiffener tip. The non-linear model also predicted the bend stiffener tip to be the critical spot.

8.2.1 On hysteresis in general

The results seem to show a significantly larger damage when the slip stiffness is used, compared to the stick stiffness. The non-linear graph seems to be positioned somewhere near the stick-stiffness. The jumper configuration results in a relatively short riser length, leading to a smaller tension force compared to other configurations, like the catenary or pliant wave configuration. One would expect the movements to be slightly larger due to this fact. For larger movements, the riser would experience more hysteresis, leading to a larger difference between the non-linear model and the linear stick-model. If these results are to give an estimate on different configurations, the damage would most likely be closer positioned to the stick-stiffness model damage.

The load cases for which the riser slips is critical to determine, as this can be used to say something about the importance of the hysteresis effect. The damage is linearly dependent on the number of waves, and it would be useful to determine the relationship between the number of waves not leading to hysteresis, and the number of waves leading to hysteresis. If it can be shown that the majority of the waves does not give non-linear behaviour, then the damage estimate can be significantly reduced by using the non-linear model, compared to using a linear-slip model.

The scenario that would lead to the largest differences between the models would be when the curvature is just under the slip curvature. This would cause much movement of the linear slip-stiffness model, but the non-linear model would always behave like a stiff pipe, leading to large differences.

8.3 Numerical problems

A time step of 0.01 for the non-linear model and 0.1 for the linear model seemed to give correct results for the curvature. The curvature history plots had a smooth, regular and predictable behaviour. Unfortunately, the forces seemed to experience larger convergence problems. The tension history had occurrences of large and sudden peaks, but apart from this it seemed to behave good. It should be noted that this was only present in some of the most severe load cases. Since the time step was already relatively low for the non-linear model and the curvature showed good behaviour, no further actions were taken. This unfavorable mistake lead to difficulties in predicting the tension variation numerically using Matlab, but a visual inspection of the curvature was carried out to see the general trend. The tension variation was therefore not presented with numerical values in the results chapter, but can be found in the appendices. The mean tension was presented, as these tension peaks not had a too large impact on this value.

The stress history was further examined to see if the numerical problems in the tension affected this. The stress graphs did not show any unpredictable behaviour or illogical values. They stresses and the fatigue damage can still be slightly influenced, but this is not believed to have a large effect on the fatigue damage. The curvature has a larger effect on the stresses than the tension force, and this had a smooth behaviour.

The only element affected by the numerical problems in the tension was element 316, which is closest to hang-off. The damage in the adjacent elements did not indicate that this should be critical spot, so this high stress level is most likely due to the numerical problems in the tension force. The unrealistically high damage in element 316 was therefore neglected, and this is why some of the plots display this element with zero damage.

Chapter 9

Conclusion

The first linear constitutive model assumed the stiffness in bending to be equal the to stiffness when the pipe is fully pressurised and no slip occurs between the layers. This model predicted the smallest dynamic response and the least fatigue damage for all the load cases. The damage was evenly spread out, and there were no clearly defined critical spot. This behaviour is as expected, due to the high stiffness causing less motion of the riser.

The second linear constitutive model assumed the bending stiffness to be equal to the stiffness when the riser is depressurised, with no friction between the tensile layers. This low stiffness resulted in the largest dynamic response and predicted the highest fatigue damage. Most of the damage was concentrated at the bend stiffener tip, which was determined to be the fatigue critical spot.

The third model took the real, non-linear behaviour of a flexible pipe into account. This model represented the stick-slip effect that occurs due to friction between the layers and pressure in pipe. This model predicted a damage about 25% greater than the linear stick-stiffness model. The linear slip-stiffness model gave a 7 times larger damage than the non-linear model. In addition, this model predicted a intuitive damage distribution, with the fatigue critical spot at the bend stiffener tip. The advantage of using this non-linear model will be greater the larger the number of waves not leading to hysteresis.

When waves propagated in 45 degrees, the motion of the riser at the bend stiffener increased. This lead to an earlier slip of the layers, compared to when waves were propagating in plane. Thus, hysteresis seems to be more critical when waves lead to motion about all axes, given that the waves are equal.

The time consumption for the linear models was of almost the same order. The main difference was between the non-linear and the linear model. The non-linear model used between 2.5-3 times longer for a full analysis, dependent on which wave types were applied. To give a realistic prediction of the long-term fatigue damage,

one option could be to perform a full blocking of the wave scatter diagram. For an one hour long simulation, it is expected that today's dedicated analysis computers would need approximately four days to complete one irregular sea-state. For a full analysis, the different sea-states can be run simultaneously on multiple cores, making it an realistic option to perform a non-linear analysis.

These results showed that the predicted damage can be significantly reduced by taking the non-linear stick-slip effect into account, compared to using the overly conservative linear slip-stiffness model. This can be applied to prove that designs, which before was deemed unviable using a linear model, is safe with respect to fatigue. This opens up for the use of lower-cost solutions while still proving the design to be safe. With the performance of today's computers, taking this stick-slip effect into account is a realistic option.

Chapter 10

Further Work

The present work has mainly been focused on how the three models behave differently when subjected to regular waves. One irregular analysis has been done, and this will not give a sufficient estimate of the damage between the three models. It is therefore proposed that the non-linear model should be studied closer with regard to how it behaves in irregular waves. This will be a more time demanding process, but the advantage is that the obtained results will give a more accurate description of the performance in real life. To get an acceptable long-term damage estimate, one should block the wave scatter diagram into a number of irregular sea states. This was intended to perform in this thesis, but due to lack of time it was not performed. This was done in agreement with the supervisor.

Two wave headings has been checked in this study, but no current or offset has been applied. To further assess the fatigue damage, it can be considered to apply a vessel offset, current and take into account more wave headings.

Using a different bend stiffener design can considered. The fatigue results showed that the damage distribution was very concentrated on the bend stiffener tip when using the linear slip model. This may either be due to a high stiffness, or the bend stiffener being too short. This would most likely spread the damage more evenly out in the linear slip model, and may make an influence on the difference between the non-linear and the linear slip-stiffness model. The different damage for these two models would most likely be less.

An equivalent viscous damping coefficient should be implemented in the linear model. This coefficient should take into account the work loss due to friction between the layers. Since this parameter is dependent on the amplitude of the motion, a possibility would be to use an amplitude so that the damping in the most critical element would be correct for the dominating wave height.

There are parts of the riser where the layers are more prone to slip. Taking the non-linear hysteresis effect into account in the first ten meters at the bend stiffener,

and use a linear stiffness on the rest of the riser could be an idea to reduce the computational time.

Since BFlex and SIMLA shares the same element library, an interesting approach would be to use BFlex elements in the global analysis. The time consumption with regard to the method used in this thesis would be of interest. This significantly simplifies the process, as the stresses in the tensile armouring can be calculated directly from the global analysis.

References

4Subsea. Design basis of jumper. Technical report containing information about configuration, weather, bend stiffener, etc, 2014.

A. Almar-Næss and et al. *Fatigue Hanbook - Offshore Steel Structures*. Tapir, 1985.

Tore Roberg Andersen. Corrosion fatigue of steel armours in flexible risers. In *International Conference on Offshore Mechanics and Arctic Engineering*, 2002.

API. *API 17B Recommended Practice for Flexible Pipe*. American Petroleum Institute, 2002.

API. *API 17J Specification for Unbonded Flexible Pipe*. American Petroleum Institute, 2008.

Yong Bai and Qiang Bai. *Subsea Pipelines and Risers*. Elsevier, 2005.

S. Berge, A. Engseth, I. Fylling, C.M. Larsen, B.J. Leira, I. Nygaard, and A. Olufsen. *Handbook on Design and Operation of Flexible Pipes*. 1992.

BMP. Bend stiffener image, April 2014. URL `http://www.subseacableprotection.com/products/bend-stiffeners.cfm`.

DNV. *DNV-OS-F201 Dynamic Risers*. DNV GL, 2010a.

DNV. *DNV-RP-F204 Riser Fatigue*. DNV GL, 2010b.

DNV. *Recommended Practice C203 - Fatigue Design of Offshore Steel Structures*. DNV GL, 2012.

O.M. Faltinsen. *Sea Loads on Ships and Offshore Structures*. Cambridge University Press, 1990.

C. A. Felippa and B. Haugen. Unified formulation of small-strain corotational finite elements. Technical report, University of Colorado, 2005.

I Kraincanic and E Kebadze. Slip initiation and progression in helical armouring layers of unbonded flexible pipes and its effect on pipe bending behaviour. *The Journal of Strain Analysis for Engineering Design*, 2001.

I. Langen and R. Sigbjornsson. *Dynamisk Analyse av Konstruksjoner*. Tapir, 1979.

Torgeir Moan. *Finite Element Modelling and Analysis of Marine Structures*. Torgeir Moan, 2003.

MSC Software, April 2014. URL `http://www.mscsoftware.com/training_videos/patran/Reverb_help/index.html#page/Fatigue%20Users%20Guide/fat_theory.15.3.html`.

Adam Nieslony. Determination of fragments of multiaxial service loading strongly influencing the fatigue of machine components. *Mechanical Systems and Signal Processing*, 2009.

Adam Nieslony and Michal Böhm. Mean stress effect correction using constant stress ratio s-n curves. *International Journal of Fatigue*, 2013.

PSA. *Unbonded Flexible Risers - Recent Field Experience and Actions for Increased Robustness*. PSA, 4Subsea, 2013.

Svein Sævik. *On Stresses and Fatigue in Flexible Pipes*. PhD thesis, NTH, Trondheim, Norway, 1992.

Svein Sævik. *SIMLA Theory Manual*. MARINTEK, 2008.

Svein Sævik. *Bflex2010 Theory Manual*, 2010.

Svein Sævik. Theoretical and experimental studies of stresses in flexible pipes. *Computers and Structures*, 2011.

Svein Sævik. *Lecture Notes in Offshore Pipeline Technology*. NTNU, 2013.

Svein Sævik. Conversations with Professor Svein Sævik. 2014.

Svein Sævik, Ole David Økland, Gro Sagli Baarholm, and Janne K. Ø. Gjøsten. *BFlex2010 Version 3.0.9 User Manual*, 2013a.

Svein Sævik, Ole David Økland, Gro Sagli Baarholm, and Janne K. Ø. Gjøsten. *SIMLA User Manual Version 3.16*. MARINTEK, 2013b.

R. Smith, F. Grealish, and J. Zimmerman. New industry guidelines for fatigue analysis of unbonded risers. In *Offshore Technology Conference*, 2007a.

Russel Smith, Tommie Carr, and Michael Lane. Computational tool for the dynamic analysis of flexible risers incorporating bending hysteresis. In *International Conference on Offshore Mechanics and Arctic Engineering*, 2007b.

Russel Smith, Patrick O'Brien, Tim O'Sullivan, and Christian Weibe. Fatigue analysis of unbonded flexible risers with irregular seas and hysteris. In *Offshore Technology Conference*, 2007c.

Nils Sødal. *Fatigue loads and fatigue load effect analysis*. DNV, 2009.

Zhimin Tan, Peter Quiggin, and Terry Sheldrake. Time domain simulation of the 3d bending hysteresis behaviour of an unbonded flexible riser. In *International Conference on Offshore Mechanics and Arctic Engineering*, 2007.

Appendix A

Fatigue Results

A.1 Regular waves in plane

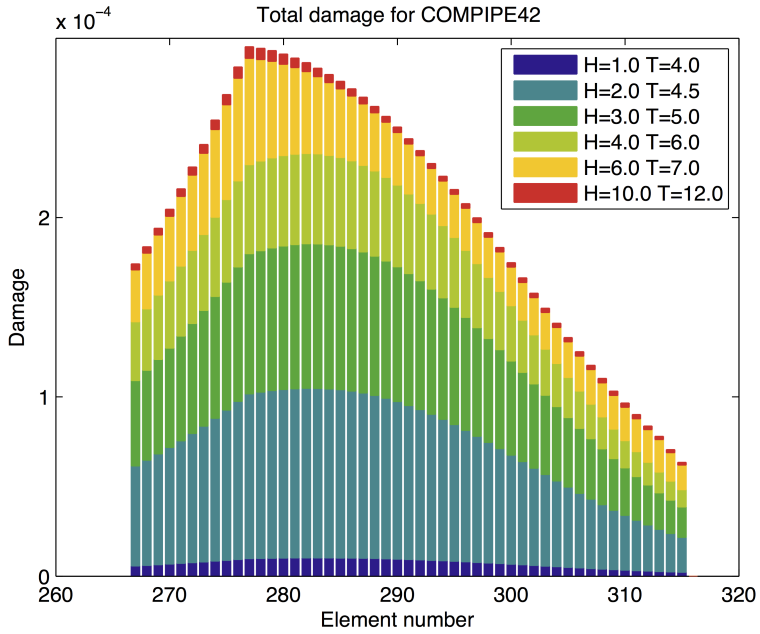

NON-LINEAR STIFFNESS

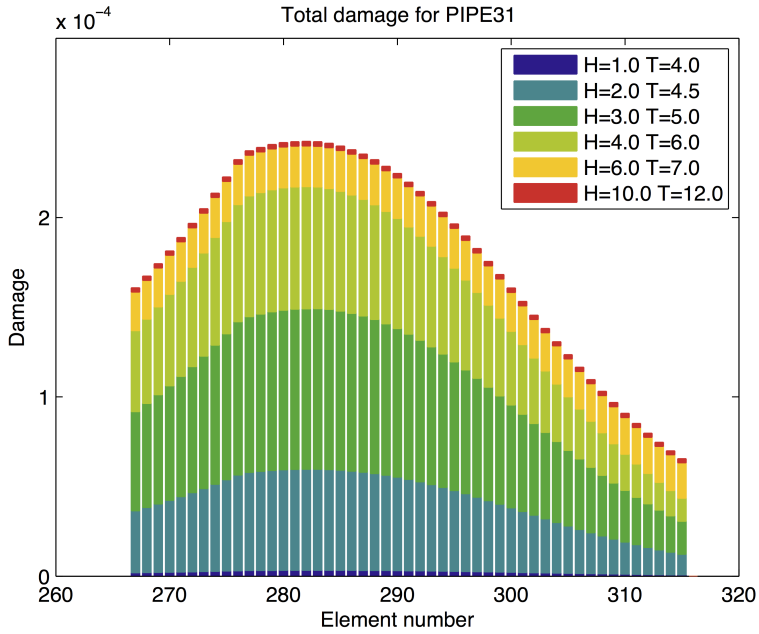

LINEAR STICK-STIFFNESS

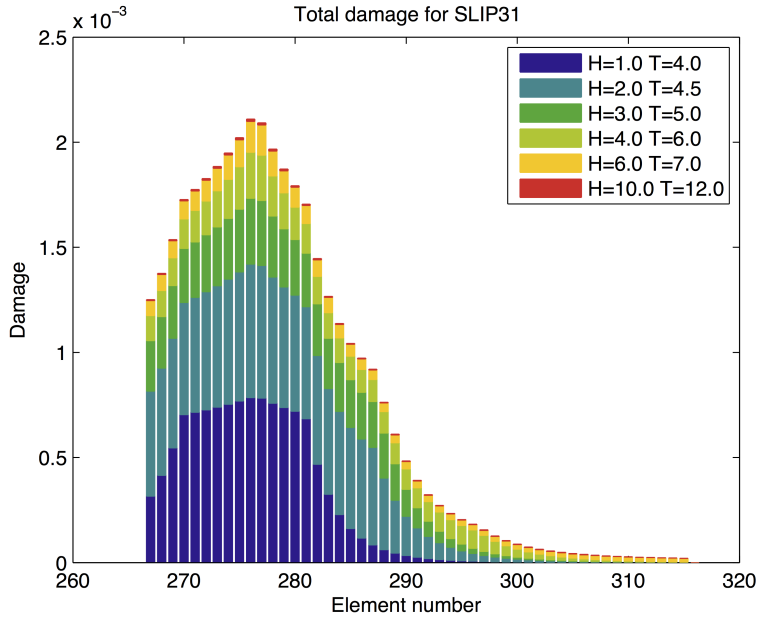

LINEAR SLIP-STIFFNESS

A.2 Regular waves, 45 degrees

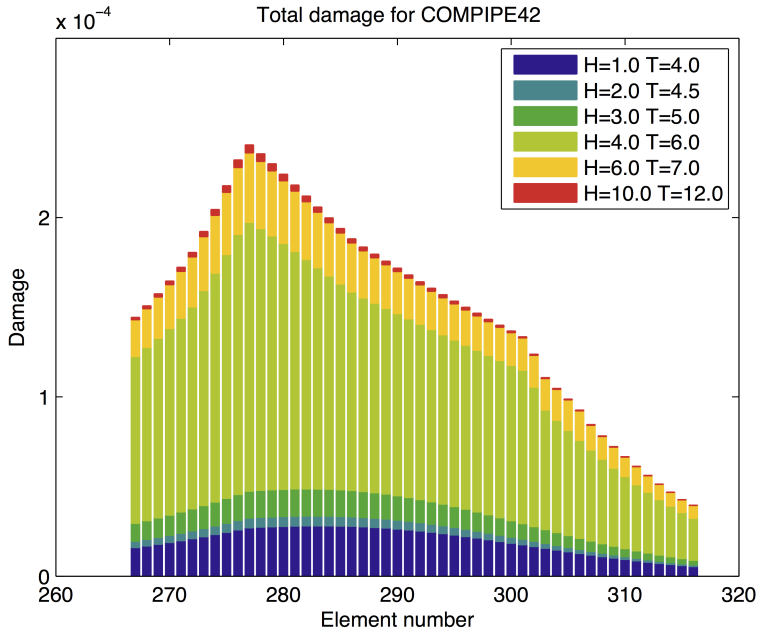

NON-LINEAR STIFFNESS

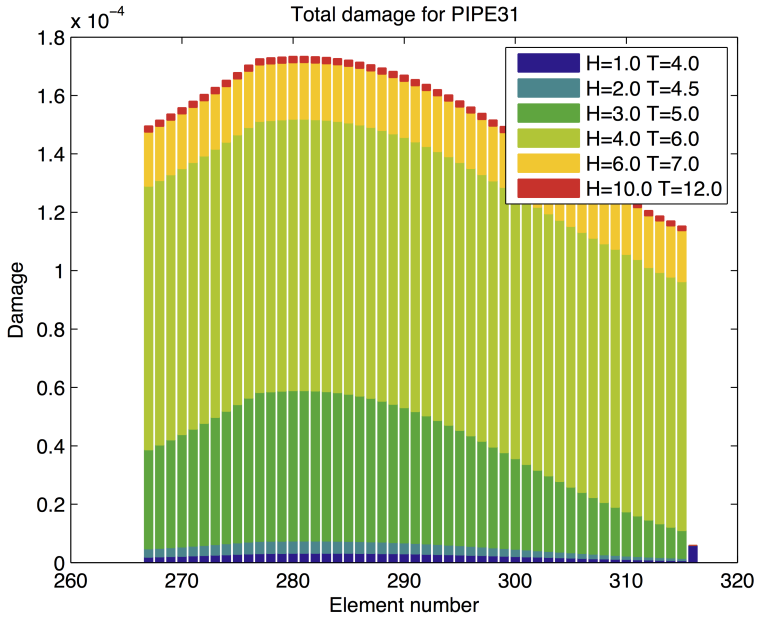

LINEAR STICK-STIFFNESS

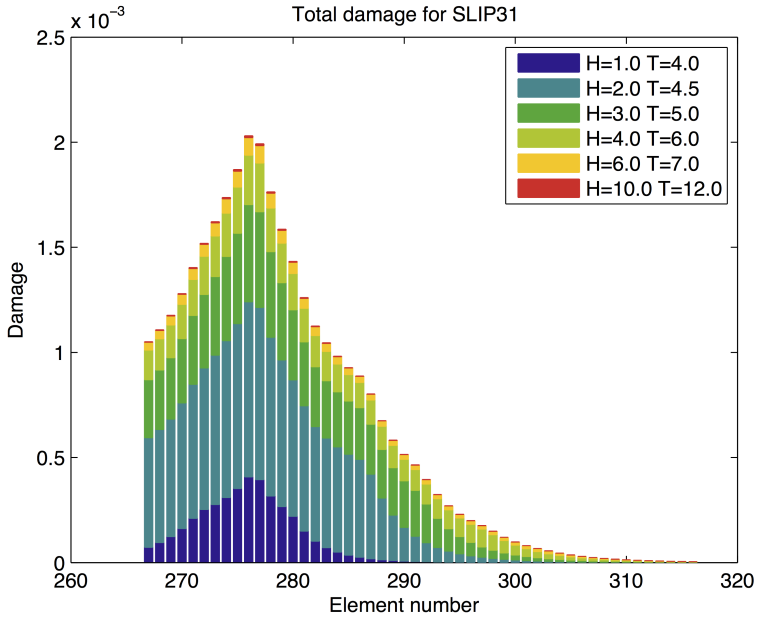

LINEAR SLIP-STIFFNESS

A.3 Irregular waves in plane

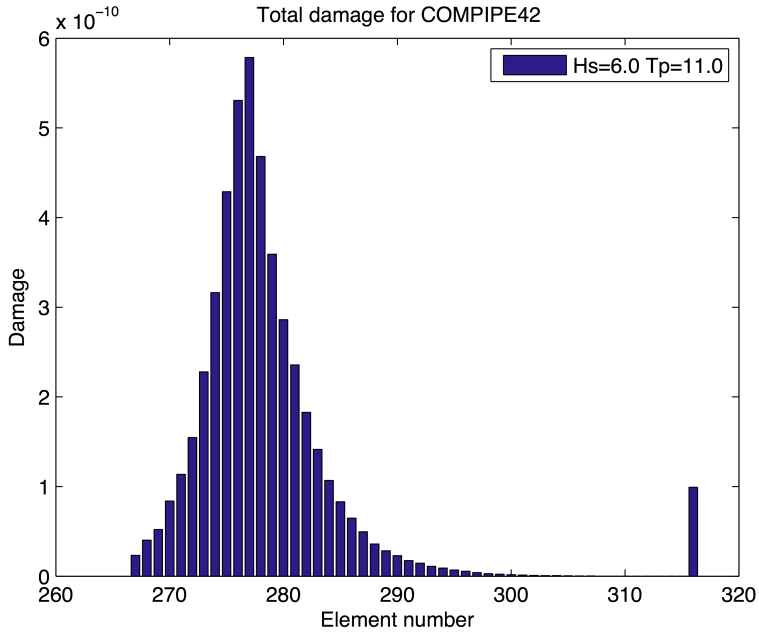

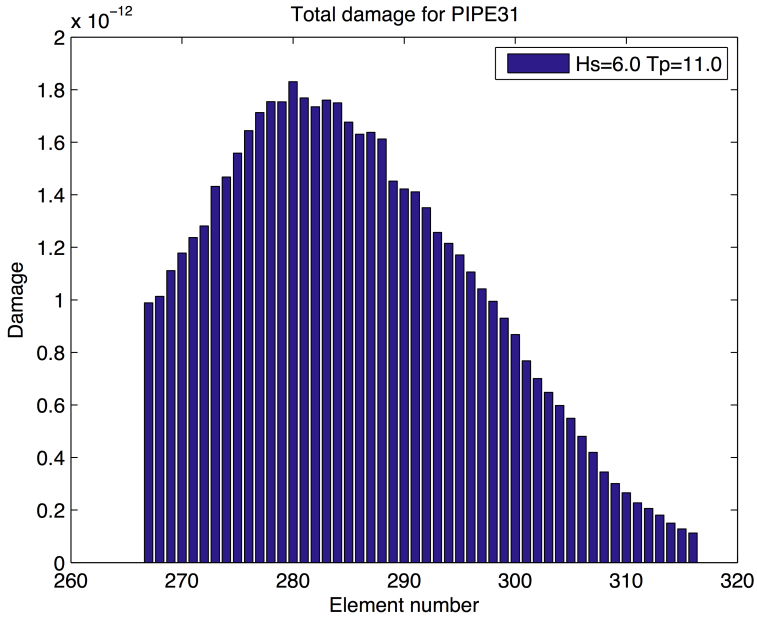

LINEAR STICK-STIFFNESS

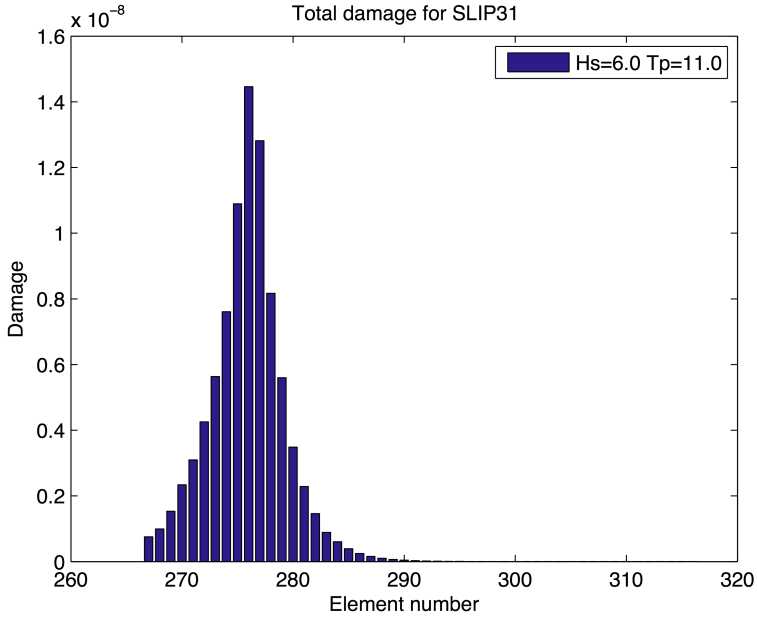

LINEAR SLIP-STIFFNESS

Appendix B

RAO

B.1 Waves in plane

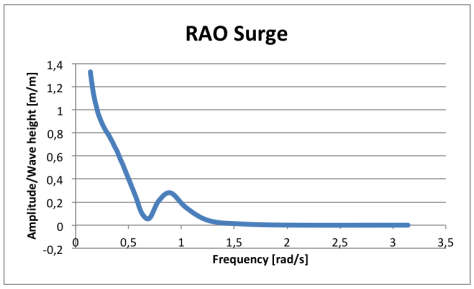

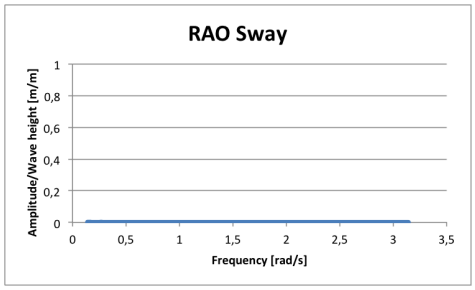

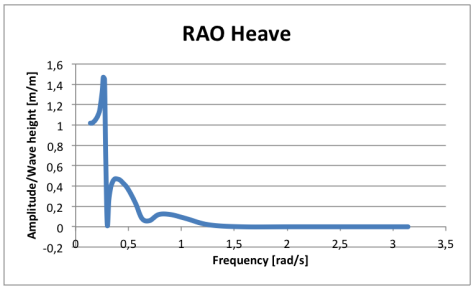

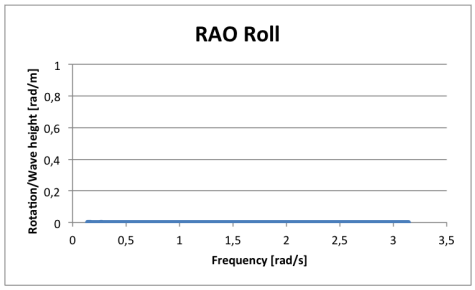

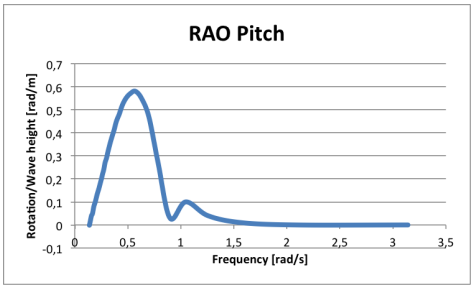

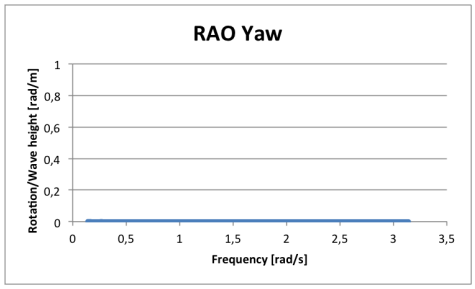

B.2 Waves heading in 45 degrees

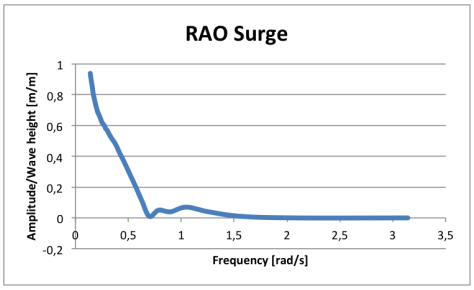

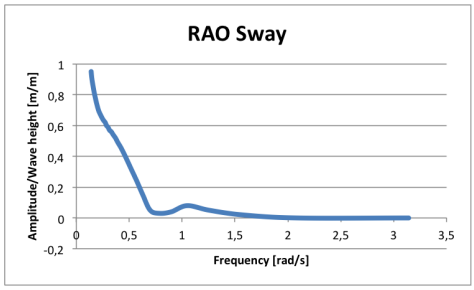

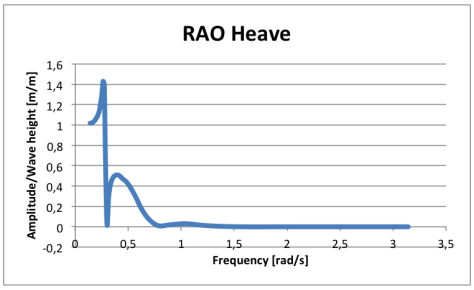

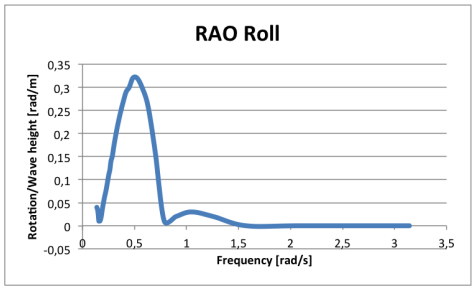

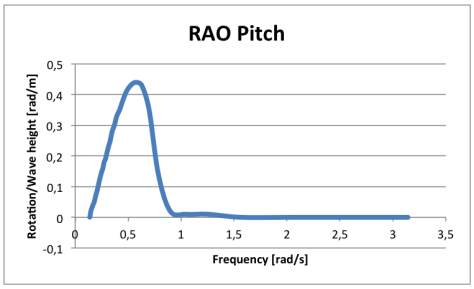
RAO Pitch
Rotation/Wave height [rad/m]
0,5
0,4
0,3
0,2
0,1
0
-0,1
0
0,5
1
1,5
2
2,5
3
3,5
Frequency [rad/s]

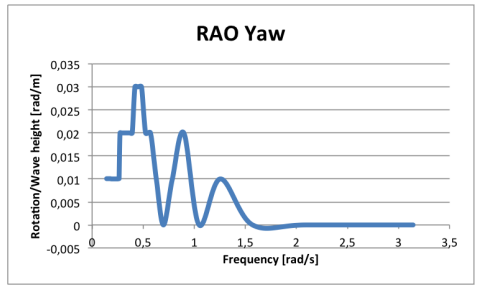
RAO Yaw
Rotation/Wave height [rad/m]
0,035
0,03
0,025
0,02
0,015
0,01
0,005
0
-0,005
0
0,5
1
1,5
2
2,5
3
3,5
Frequency [rad/s]